LICENSING REPORT ON
HIGH DENSITY
SPENT FUEL RACKS

FOR

QUAD CITIES PROJECT

OAT J-2443

COMMONWEALTH EDISON P.O. #249405

BY

K.P. SINGH, Ph.D.
VICE PRESIDENT, ENGINEERING
JOSEPH OAT CORPORATION

AND

STANLEY TURNER, Ph.D.
VICE PRESIDENT
SOUTHERN SCIENCE APPLICATIONS, INC.

REPORT TM-600

TABLE OF CONTENTS

		Page
1.	PREFACE	1.1
2.	GENERAL ARRANGEMENT	2.1
3.	RACK CONSTRUCTION	3.1
	References to Section 3	3.3
4.	NUCLEAR CRITICALITY ANALYSIS	4.1
	4.1 Design Bases	4.1
	4.2 Geometric and Calculational Models	4.3
	4.2.1 Reference Fuel Assembly	4.3
	4.2.2 Alternative Fuel Assembly Designs	4.3
	4.2.3 Calculational Models	4.7
	4.2.3.1 Analytical Methods	4.7
	4.2.3.2 Calculational Bias and Uncertainty	4.9
	4.2.3.3 Trend Analysis	4.9
	4.2.4 Reference Fuel Storage Cell	4.10
	4.3 Reference Subcriticality and Mechanical Tolerance Variations	4.11
	4.3.1 Nominal Case	4.11
	4.3.2 Alternative Fuel Assemblies	4.11
	4.3.3 Boron Loading Variation	4.11
	4.3.4 Storage Cell Lattice Pitch Variation	4.13
	4.3.5 Stainless Steel Thickness Variations	4.13
	4.3.6 Fuel Enrichment and Density Variation	4.15
	4.3.7 Boraflex Width Tolerance Variation	4.15
	4.3.8 Effect of Zirconium Fuel Channel	4.15
	4.4 Abnormal and Accident Conditions	4.17
	4.4.1 Fuel Assembly Positioning in Storage Rack	4.17
	4.4.2 Effect of Zirconium Flow Channel Distortion	4.17
	4.4.3 Temperature and Water Density Effects	4.18
	4.4.4 Abnormal Positioning of Fuel Assembly Outside Storage Rack	4.18
	4.4.5 Missing Absorber Plate	4.19
	4.4.6 Dropped Fuel Assembly Accident	4.19
	4.4.7 Fuel Rack Lateral Movement	4.21
	4.5 Summary	4.22
	References	4.24
5.	HYDRO-THERMAL CONSIDERATIONS	5.1
	5.1 Heat Generation Calculations (Later)	5.1
	5.2 Analysis of Pool Thermal-Hydraulics	5.2

References 5.4

6. SEISMIC ANALYSIS 6.1

6.1 Analysis Outline 6.1
6.2 Fuel Rack - Fuel Assembly Model 6.3

6.2.1 Assumptions 6.3
6.2.2 Model Description 6.4
6.2.3 Fluid Coupling 6.5
6.2.4 Damping 6.6
6.2.5 Impact 6.7

6.3 Stress Analysis 6.8

6.3.1 Stiffness Characteristics 6.8
6.3.2 Combined Stresses and Corner Displacements 6.9

6.4 Time Integration of the Equations of Motion 6.11

6.5 Structural Acceptance Criteria 6.13

References 6.24

7. MISCELLANEOUS ANALYSES 7.1

8. RADIOCHEMICAL ANALYSES (Later) 8.1

8.1 Objective and Assumptions 8.1

8.2 Method of Analysis 8.3

References 8.4

9. POOL STRUCTURAL CALCULATIONS (Later)

10. NEUTRON ABSORBER MATERIAL 10.1

10.1 Chemical Composition 10.1

10.2 Physical Properties 10.2

11. IN-SERVICE SURVEILLANCE PROGRAM FOR BORAFLEX NEUTRON ABSORBING MATERIAL 11.1

1. PREFACE

Quad-Cities Nuclear Power Station consists of two (2) generating units (Unit 1 and Unit 2), each with a General Electric BWR-3 Reactor. The station is owned by Commonwealth Edison Company (65%) and Iowa-Illinois Gas and Electric Company (25%), and is operated by Commonwealth Edison Company. The two utilities share the electrical output in proportion to the ownership.

The station will loose full core discharge capability at the Fall 1981 Unit 2 refueling outage. A limited number of unused fuel racks of the original design are available to be installed, which could extend the date for loss of full core discharge capability to the Fall of 1982. No further extension is currently possible.

Commonwealth Edison Company, in its function as operator, proposes to increase the spent fuel storage capacity by replacing the present spent fuel storage racks with new high density storage racks. This modification will include use of a neutron absorber material in the racks, as an increase of Keff from 0.90 to 0.95.

The specification for design, construction and quality assurance of the high density racks, was prepared by Quadrex, a San Jose based company. The mechanical design, seismic analysis, hydrothermal analysis and other related calculations as well as fabrication of the hardware will be performed by Joseph Oat Corporation. Joseph Oat Corporation, based in Camden, N.J., possesses ASME Code stamps for Section III, Class 1, 2, 3 and MC pressure vessels and components. Oat also has a qualified Q.A. program in accordance with 10CFR 50 Appendix B.

Southern Science Applications, Inc. of Dunedon, Florida, is serving as a consultant to Joseph Oat Corporation in the areas of criticality analysis and other radionuclide evaluations. Southern Science has a qualified Q.A. System audited and accepted by the Q.A. division of Joseph Oat Corporation.

Consulting support on the overall effort is provided by NUS Corporation of Rockville, Maryland.

2. GENERAL ARRANGEMENT

Quad-Cities Units 1 and 2 each possess fuel storage pools 33' wide x 41' long. The high density racks described in this Report are engineered to achieve the dual objective of maximum protection against structural loadings (such as ground motion) and maximization of available storage locations. Greater width to height aspect ratio provides greater margin against rigid body tipping. Hence, the modules are made as large as possible within the constraints of transportation and site handling capabilities.

Quad-Cities Unit 1 pool will contain high density fuel racks in 8 different module sizes. The module types are labelled A through H in Figure 2.1, which also shows their relative placement. There will be a total of 3,657 storage locations in the Quad-Cities Unit 1 pool.

Quad-Cities Unit 2 pool will contain 3,913 storage cells arranged in 20 racks. There will be 7 different module types in this pool. Figure 2.2 shows the module placement details with respect to the pool inside boundary.

Table 2.1 gives the detailed module data, e.g., weight, quantity and number of storage locations.

All modules are free standing, i.e., they are not anchored to the pool floor or connected to the pool wall through snubbers or lateral restraints. The minimum gap between adjacent racks is 3.5" at all locations. Sufficient gap is also maintained between the modules and the pool walls. The minimum gap between the fuel pool wall and rack modules is 7½" (ref. Figure 2.1). Adequate clearance from other pool resident hardware is also provided. Due to the gaps provided, the possibility of inter-rack impact, or rack collision with other pool hardware during the postulated ground motion events is precluded.

TABLE 2.1 MODULE DATA

Type	QUANTITY	NO. OF CELLS/MODULE	CELLS N.S. DIRECTION	CELLS E.W. DIRECTION	APPROX. WEIGHT LBS/MODULE	COMMENTS
A	12	210	15	14	27,000	Rectangular Modules
B	6	196	14	14	25,500	Square Modules
C	8	182	14	13	17,000	Rectangular Modules
D	2	169	13	13	22,000	Square Modules
E	4	120	15	8	15,500	Rectangular Modules
F	2	256	16	16	33,300	Square Modules
G	4	224	16	14	29,000	Rectangular Modules
H	1	192	16	12	25,000	Rectangular Modules

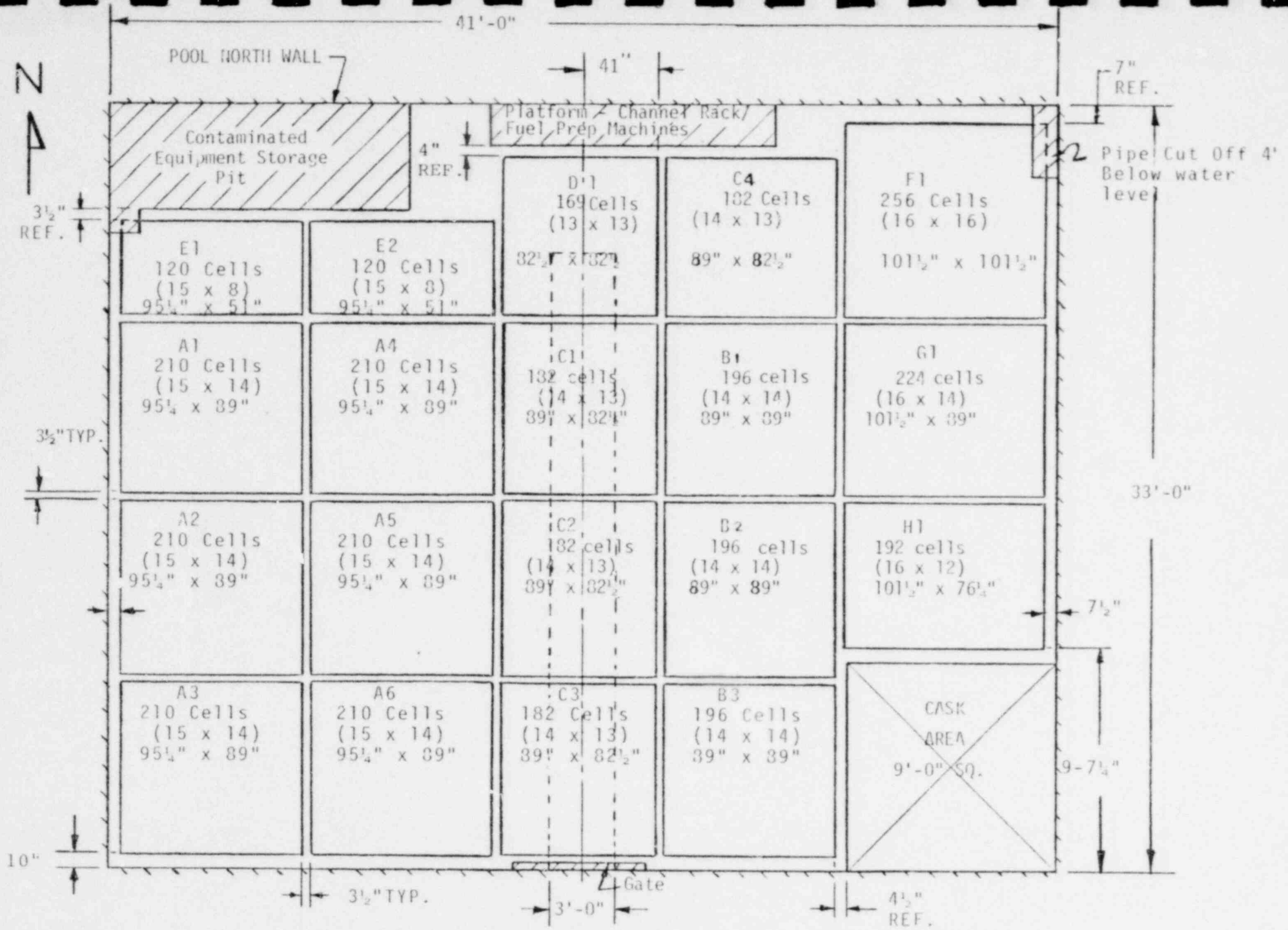

Fig. 2.1 RACK MODULES ARRANGEMENT QUAD-CITIES UNIT 1 - (3657 Cells)

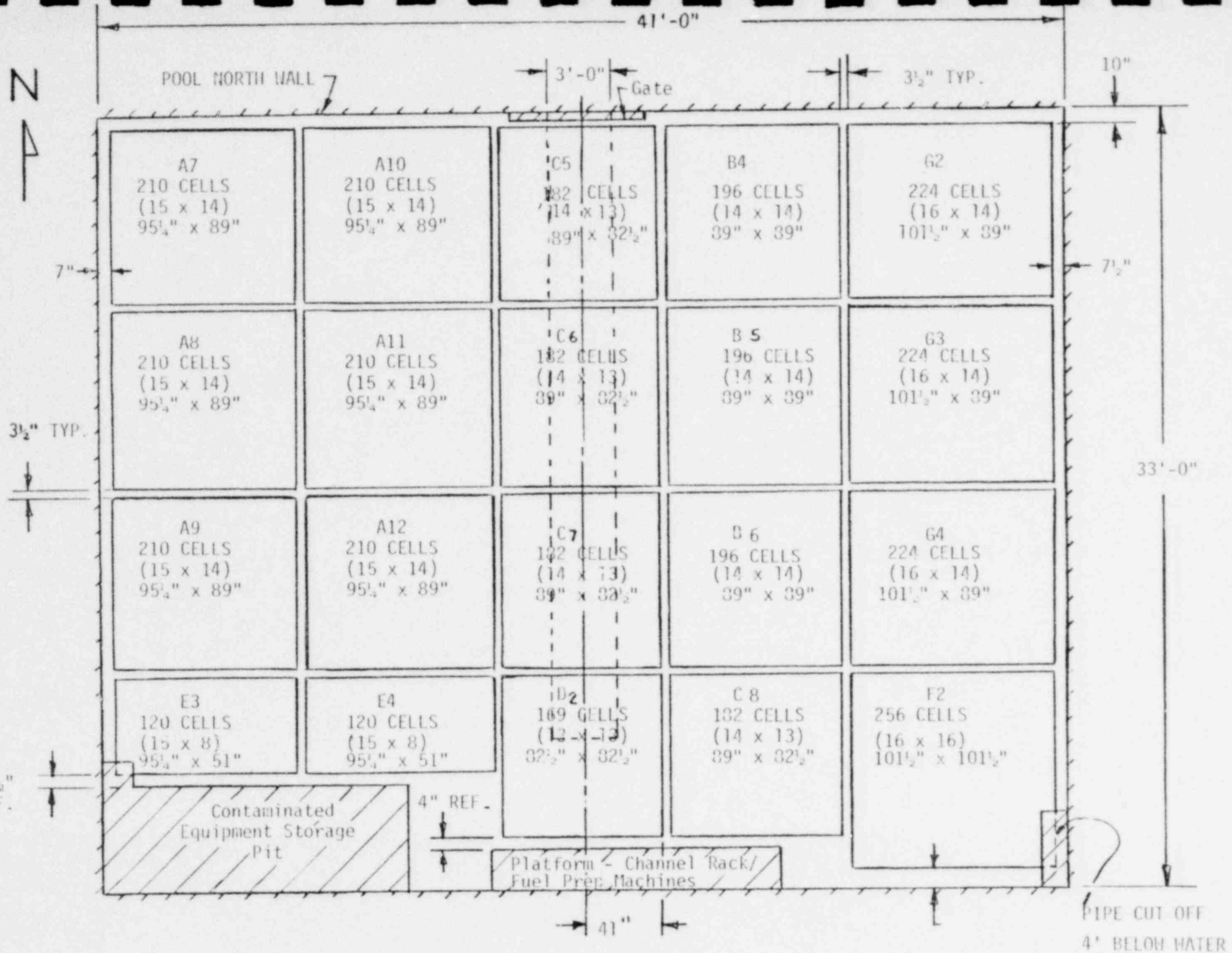

Fig. 2.2RACK MODULES ARRANGEMENT QUAD-CITIES UNIT 2 - (3913 CELLS)

3. RACK CONSTRUCTION

The racks will be constructed from ASTM 240-304, austenitic steel sheet material, ASTM 204-304 austenitic steel plate material, and ASTM 182-F304 austenitic steel forging material. Boraflex, a patented brand name product of Bisco* will serve as the nuetron absorber material. The detailed radiological properties of Broaflex may be found in Section 4 and Section 10.

A typical module will contain storage cells which have 6" minimum internal cross-sectional opening. These cells will be straight to within $\pm$0.125". These dimensions ensure that fuel assemblies with maximum permissible channel deformations can be inserted into the storage cells.

Figure 3.1 shows a horizontal cross-section of an array of 3 x 3 cells. The cells provide a smooth and continuous surface for lateral contact with the fuel assembly. The construction of the rack modules may best be described by exposing the basic building blocks of this design, namely the "cruciform", "ell" and "tee" elements, shown in Figure 3.2. The cruciform element is made of 4 angular sub-elements, "A" (Figure 3.3) with the neutron absorber material tightly sandwiched between the stainless sheets. The cruciform assembly has 5" high stainless strips, which ensure against slippage of the "poison" material downwards due to gravitation loads or operating conditions. The fabrication procedure leads to 100% surface contact (in macroscopic sense) between the poison and the stainless sheets. The top of the cruciform is also end welded using a spacer strip as shown in Figure 3.4. Skip welding at the top ensures proper venting of the sandwiched space in the cruciform spokes.

The "ell" and "tee" elements are constructed similarly using angular sub-element "B", and flat sub-element "C" (Figure 3.5). Having fabricated the required quantities of the "cruciform", "tees" and "ells", the assembly is performed in a specially designed fixture which serves the function of maintaining dimensional accuracy while

* Bisco, a Division of Brand, Inc., 1420 Renaissance Drive, Park Ridge, Illinois

welding all the contiguous spokes of all elements using fillet welds. Figure 3.6 shows the fillet welds in a 4 x 4 array. In this manner, the cells are produced which are bonded to each other along their long edges, thus in effect, forming an "egg-crate".

The bottom ends of the cell walls are welded to the base plate which has 5.25" diameter holes concentric with cell center lines. Machined sleeve elements are positioned in the base plate and attached to the base plate through circular fillet welds (Figure 3.7). The conical machined surface on the sleeve provides a contoured seating surface for the "nose" of the fuel assembly. Thus, the contact stresses at the fuel assembly nose bearing surface are minimized.

The central hole in the sleeve provides the coolant flow path for heat transport from the fuel assembly cladding. Lateral holes in the cell walls (Figure 3.7) provide the redundant flow path in the unlikely event that the main coolant flow path is clogged.

The rack assembly is typically supported on four plate type supports. The supports elevate the module base plate 6.5" above the pool floor level, thus creating the water plenum for coolant flow.

REFERENCES TO SECTION 3

1. Oat drawing D-7070, "Fuel Cell Details", Joseph Oat Corporation, Jan, 1981.

2. Oat drawing D-7071, "Elements of Cell", Joseph Oat Corporation, Jan., 1981.

3. Oat drawing D-7072, "General Arrangement and Assembly", Joseph Oat Corporation, Jan., 1981.

4. Oat drawing D-7073, "Fixed Support Detail", Joseph Oat Corporation, Jan., 1981.

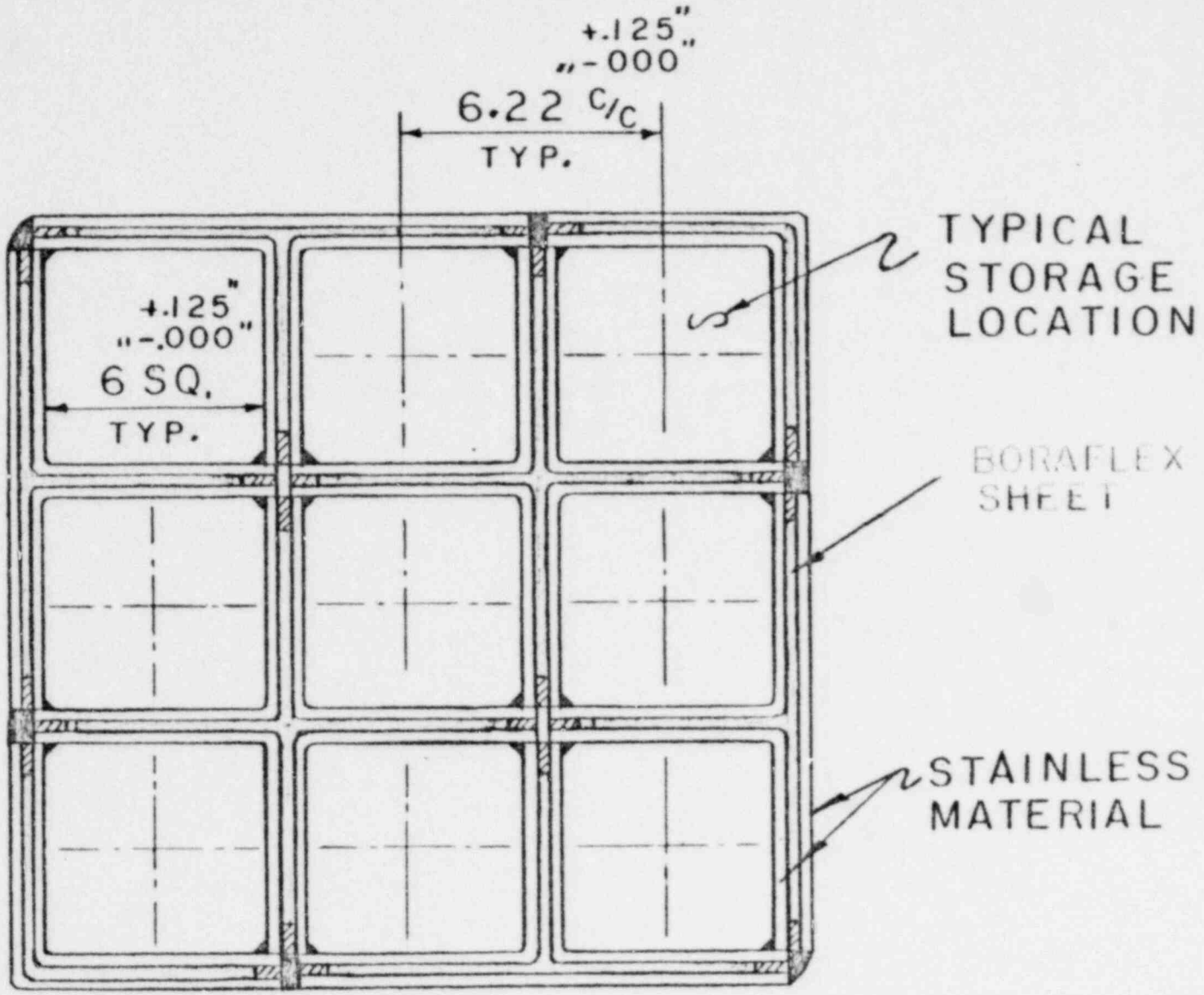

FIG. 3.1 ARRAY OF CELLS (3 X 3)

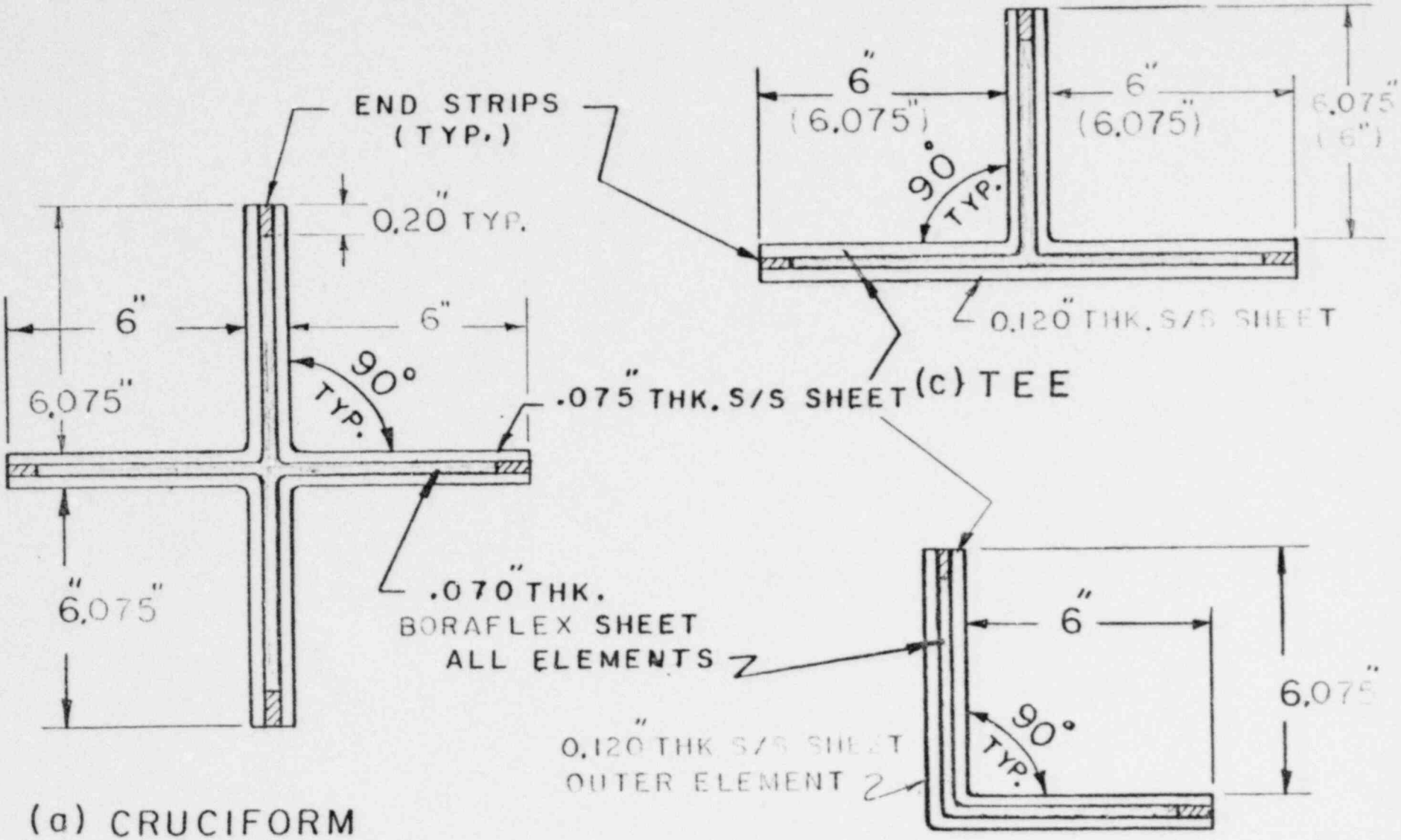

FIG. 3.2 ELEMENTS CROSS SECTION

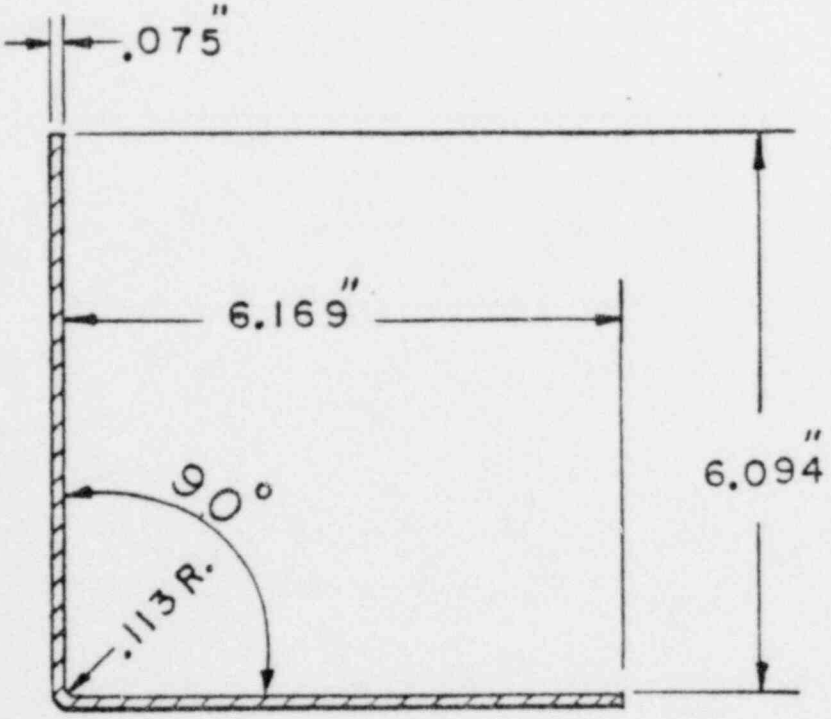

FIG. 3.3 ANGULAR
SUB ELEMENT 'A'

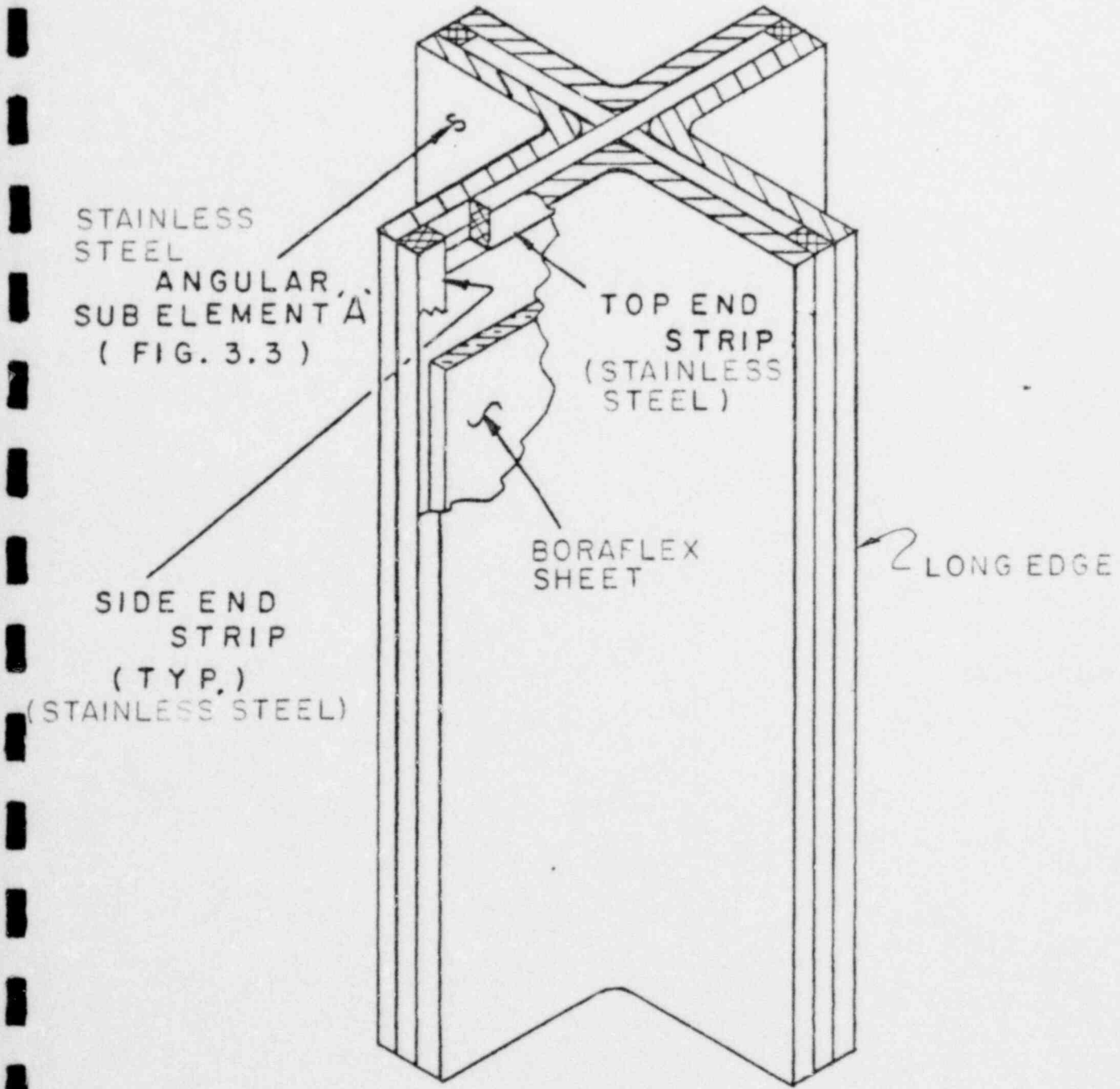

FIG. 3.4 CRUCIFORM ELEMENT
(ISOMETRIC VIEW)

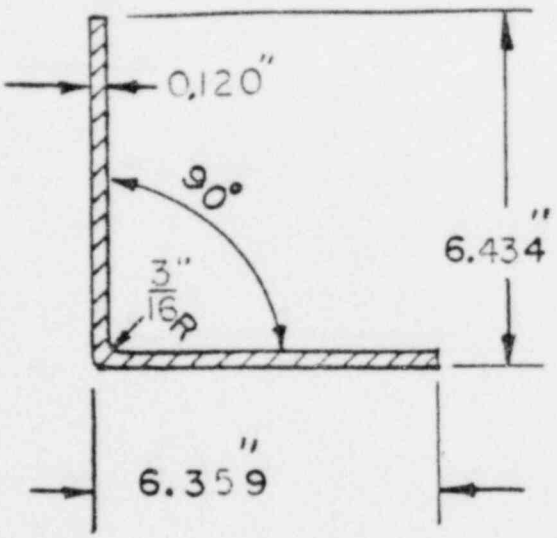

(a) ANGULAR SUB ELEMENT 'B'

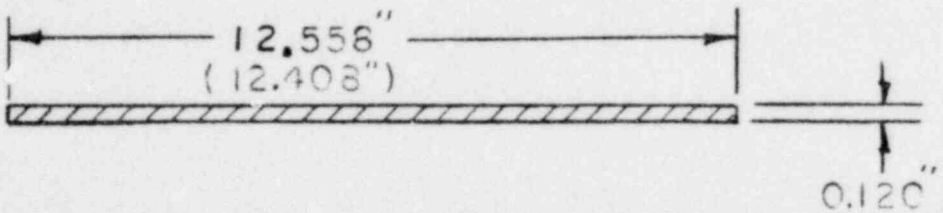

(b) FLAT SUB ELEMENT 'C'

FIG. 3.5 SUB ELEMENTS

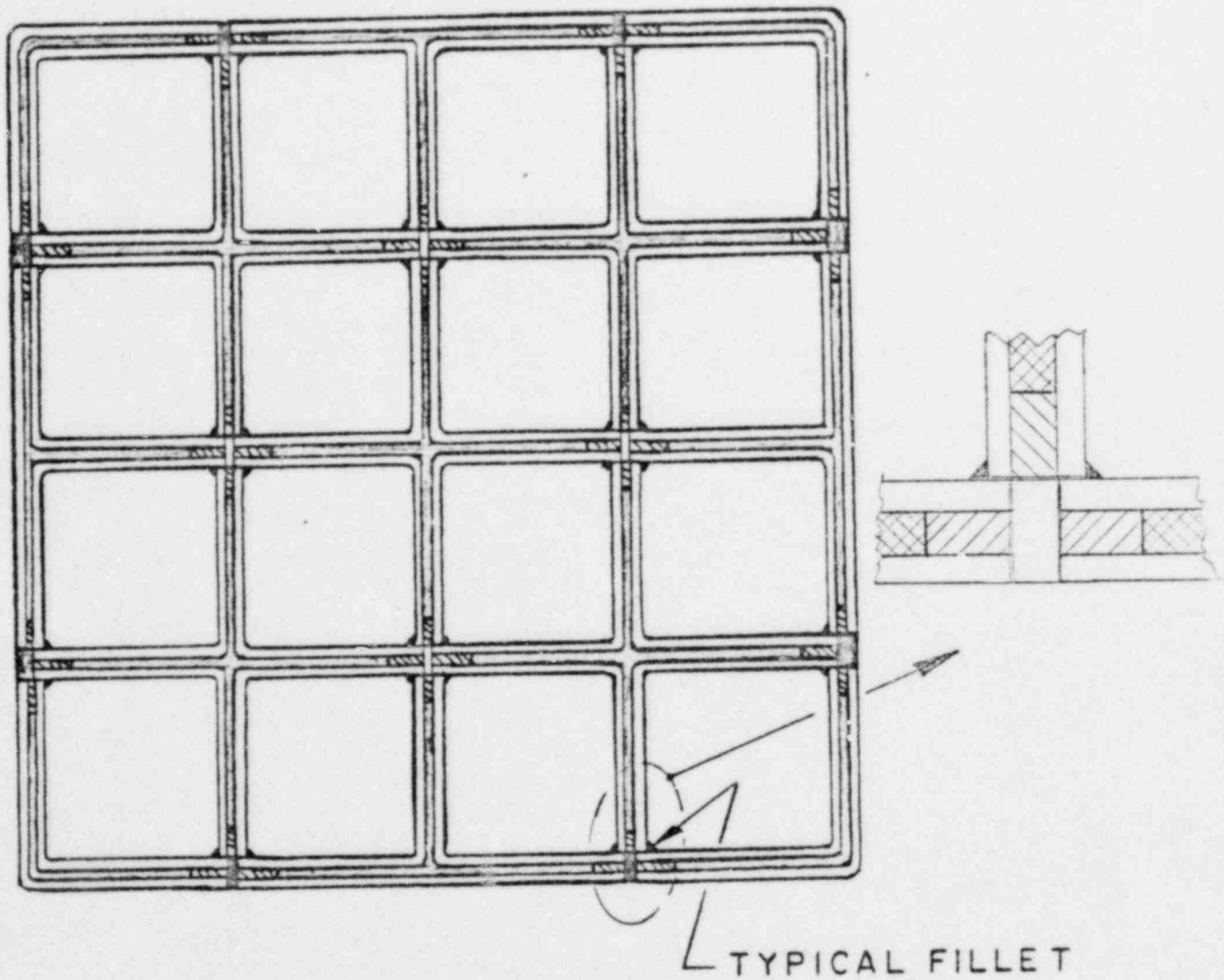

FIG. 3.6 FILLET WELD IN A 4 X 4 ARRAY

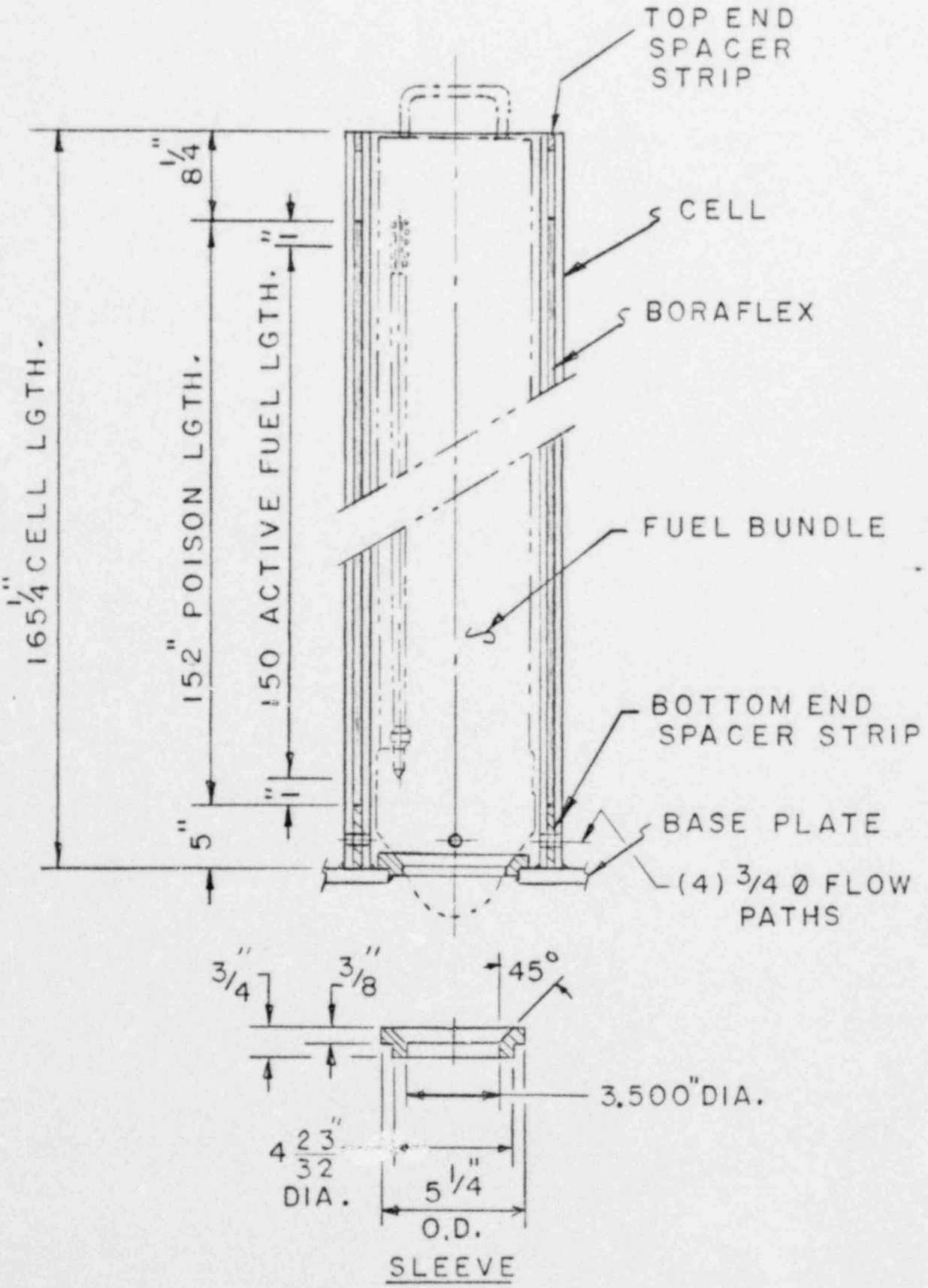

FIG. 3.7 TYPICAL CELL ELEVATION

4. NUCLEAR CRITICALITY ANALYSIS

4.1 Design Bases

The spent fuel storage racks are designed to assure that a k_{eff} equal to or less than 0.95 is maintained with the racks fully loaded with fuel of the highest anticipated reactivity and flooded with unborated water at a temperature corresponding to the highest reactivity. The maximum calculated reactivity includes a margin for uncertainty in reactivity calculations and in mechanical tolerances, statistically combined, such that the true k_{eff} will be equal to or less than 0.95 with a 95% probability at a 95% confidence level.

Applicable codes, standards and regulations or pertinent sections thereof include the following:

- General Design Criterion 62 - Prevention of Criticality in Fuel Storage and Handling.
- NRC letter of April 14, 1978, to all Power Reactor Licensees - OT Position for Review and Acceptance of Spent Fuel Storage and Handling Applications, including modification letter dated January 18, 1979.
- NRC Standard Review Plan, Section 3.8.4 and 9.1.2 as they apply to spent fuel racks.
- Regulatory Guide 3.41, Validation of Calculational Method for Nuclear Criticality Safety (and related ANSI N16.9-1975).
- ANSI N210-1976, Design Objectives for Light Water Reactor Spent Fuel Storage Facilities at Nuclear Power Plants.
- ANSI N18.2-1973, Nuclear Safety Criteria for the Design of Stationary Pressurized Water Reactor Plants.

The design basis fuel assembly is an 8 x 8 array of fuel rods (BWR type) containing UO_2 at a maximum uniform enrichment of 3.2% U-235 by weight, corresponding to 15.49 grams U-235 per axial

centimeter of fuel assembly. Fuel assemblies containing gadolinium burnable poison or assemblies of other configurations or enrichments, e.g., 7 x 7 array, may also be safely accommodated in the spent fuel storage racks provided the maximum reactivity is less than or equal to the reactivity of the design basis fuel assembly.

To assure the true reactivity will always be less than the calculated reactivity, the following conservative assumptions were made:

- Moderator is pure, unborated water at a temperature corresponding to the highest reactivity.
- Lattice of storage racks is infinite in all directions; i.e., no credit is taken for axial or radial neutron leakage.
- Neutron absorption in minor structural members is neglected; i.e., spacers and Inconel springs are replaced by water.
- Pure zirconium is used for cladding and flow channel; i.e., higher neutron absorption of alloying materials in Zircaloy is neglected.
- The spent fuel storage rack will accomodate, with the required subcriticality, fuel assemblies with maximum expected distortion of the Zr flow channel.

4.2 Geometric and Calculational Models

4.2.1 Reference Fuel Assembly

The reference design basis fuel assembly, illustrated in Fig. 4.1, is an 8 x 8 array of fuel rods with two of the central rods replaced by zirconium "water-rods." The square Zircaloy channel surrounding the fuel is 0.080 inches thick and 5.438 inches outside dimension. A maximum uniform U-235 enrichment of 3.2% U-235 by weight was assumed as the design basis corresponding to an average axial loading of 15.49 grams U-235 per axial centimeter in each fuel assembly.

The maximum expected distortion of the Zr channel is illustrated in Fig. 4.2, which is taken from GE Specification 22A5866, Rev. 0. Since the curved surface of the bulged Zr channel cannot be adequately described in the two-dimensional computer codes used for analysis, an approximation, preserving the Zr thickness and weight, was necessary as shown by the dotted lines in Fig. 4.1. This should represent a reasonable approximation, since the reactivity effect due to bulging of the Zr channel is small (see Section 4.3.8).

4.2.2 Alternative Fuel Assembly Designs

The spent fuel storage racks are also intended to accommodate fuel assemblies consisting of a 7 x 7 array and an 8 x 8 array, both containing fuel with enrichment less than 3.2% U-235 by weight. Specifications for these fuel assemblies and for the reference fuel assembly are listed in Table 4-1, which permits comparisons of the designs. The reactivity of the alternative fuel assemblies is lower than the reactivity of the design basis fuel assembly, primarily because of the lower enrichments in the alternative assemblies. Consequently, the design basis fuel assembly is the assembly of highest anticipated reactivity and is the limiting case.

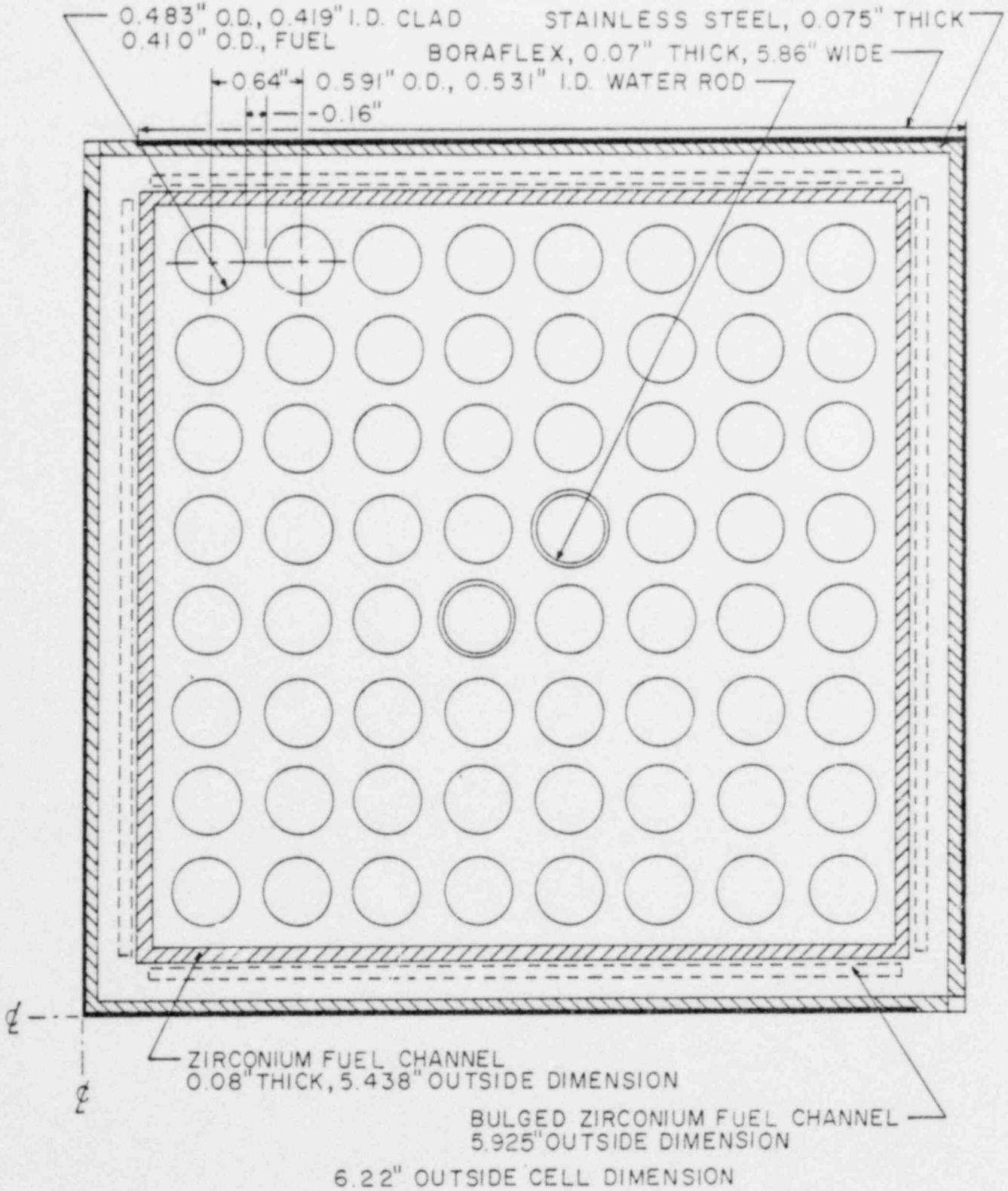

Fig. 4.1 Geometric model of Quad Cities spent fuel storage rack cell.

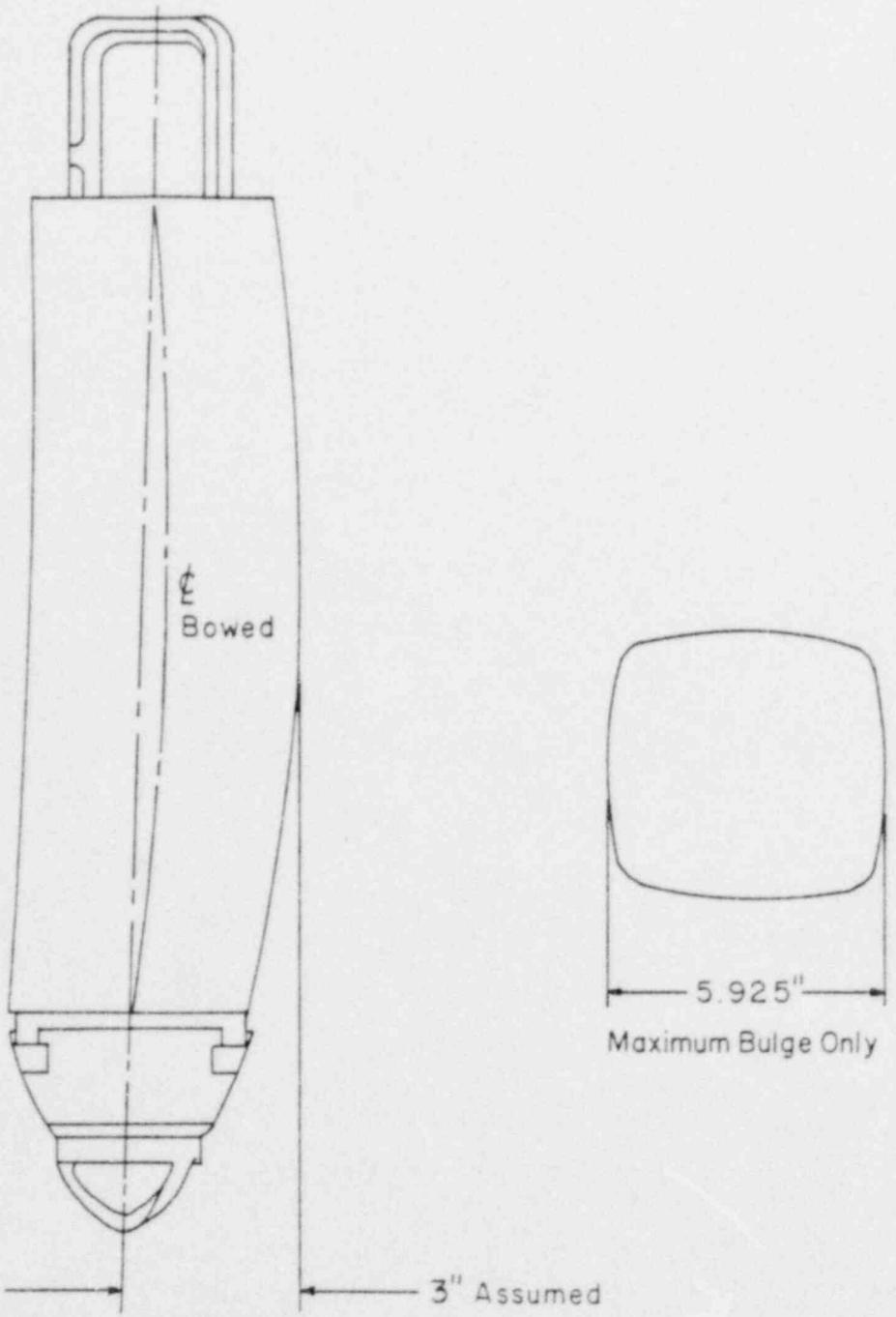

Fig. 4.2 Maximum expected distortions of a standard BWR fuel assembly (from GE Specification 22A5866, Rev. 0).

Table 4-1 FUEL ASSEMBLY DESIGN SPECIFICATIONS

	Fuel Assembly Designation		
	8 x 8R (Reference)	7x7/7x7R	8x8
Fuel Rod Data			
Outside diameter, in.	0.483	0.563	0.493
Cladding thickness, in.	0.032	0.032/0.037	0.034
Cladding material	Zr-2	Zr-2	Zr-2
Pellet density, %T.D.	95	93/95	95
Pellet diameter, in.	0.410	0.488/0.477	0.416
Enrichment, wt% U-235	3.2*	2.12/2.30	2.62
Grams U-235 per axial cm	15.49	11.25/12.46	13.26
Water Rod Data			
Outside diameter, in.	0.591	-	0.493
Wall thickness	0.030	-	0.034
Material	Zr-2	-	Zr-2
Number per assembly	2	none	1
Fuel Assembly Data			
Number of fuel rods	62	49	63
Fuel rod pitch, in.	0.640	0.738	0.640
Fuel channel outside dimension, in.	5.438	5.438	5.438
Fuel channel wall thickness, in.	0.080	0.080	0.080
Fuel channel material	Zr-4	Zr-4	Zr-4

*6 inches of natural uranium at both ends of fuel rod.

In the present analysis, gadolinium burnable poison is not included in the fuel. However, the spent fuel storage racks can safely accommodate gadolinium-bearing fuel of higher U-235 enrichment than that specified for the design basis, provided the reactivity of the fuel assembly is less than or equal to that of the reference design basis fuel assembly. For comparison purposes, the calculated reactivity (by AMPX-KENO, see Section 4.2.3 below) of the design basis fuel assembly on a 6.00-inch lattice spacing is 1.362 ± 0.004 (1σ) with unborated water in the standard reactor core geometry (see Fig. 4.3).

4.2.3 Calculational Models

4.2.3.1 Analytical Methods

Nuclear criticality analyses of the high density spent fuel storage rack were performed with the AMPX[1]-KENO[2] computer package, using the 123-group XSDRN cross-section set and the NITAWL subroutine for U-238 resonance shielding effects (Nordheim integral treatment). AMPX-KENO has been extensively benchmarked against a number of critical experiments (e.g., Refs. 3, 4, and 5).

For investigation of small reactivity effects (e.g., mechanical tolerances), a four-group diffusion/blackness theory method of analysis (NULIF-CNROD-PDQ7) was used (Ref. 5) to calculate small incremental reactivity changes. This model has been used previously with good results and is normally used only to evaluate trends and small incremental reactivity effects that would otherwise be lost in the KENO statistical variation. Where possible, trends calculated by AMPX-KENO and by diffusion/blackness theory were compared and found to be in good agreement, well within the statistical uncertainty of KENO calculations.

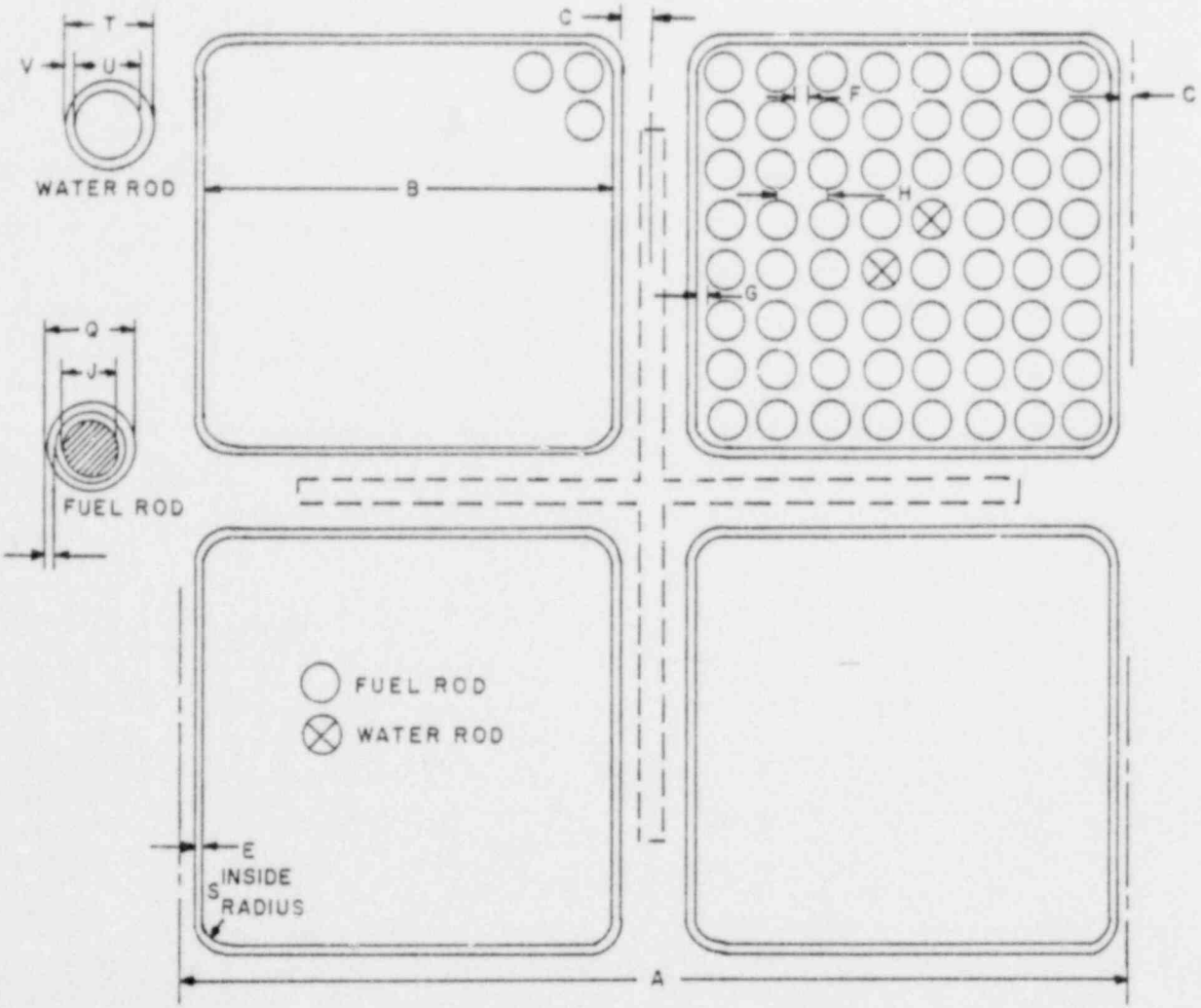

DIM. IDENT.	A	B	C	D	E	F	G	H
DIM. INCHES	12.0	5.278	0.261		0.080	0.157	0.1575	0.640

DIM. IDENT.	I	J	K	L	M	N	O	P
DIM. INCHES	0.032	0.410						

DIM. IDENT.	Q	R	S	T	U	V
DIM. INCHES	0.433		0.380	0.591	0.531	0.030

Fig. 4.3 Typical core configuration of BWR-type fuel assemblies as used in the Quad Cities reactor.

4.2.3.2 Calculational Bias and Uncertainty

Results of benchmark calculations[5] on a series of critical experiments indicate a calculational bias of 0, with an uncertainty of ±0.0123 (95% probability at a 95% confidence level). In addition, a small correction in the calculational bias is necessary to account for the slightly larger gap thickness (1.1 inches) between fuel assemblies in the Quad Cities spent fuel rack compared to the corresponding thickness (0.644 inches) in the benchmark critical experiments. Based upon the correlation developed in Ref. 5, the correction for water-gap thickness in the Quad Cities spent fuel storage rack is -0.0036 Δk (underprediction). Thus, the net calculational bias is 0.0036 ± 0.0123, including the effect of the water-gap thickness.

4.2.3.3 Trend Analysis

Trend analysis[5] of benchmark calculations on critical experiments with varying boron content in the absorber plate between fuel assemblies indicates a tendency to overpredict k_{eff} with higher reactivity worth of the boron absorber. In the Quad Cities spent fuel rack, the boron worth is about 40% Δk, or ~2.7 times the highest boron worth (15.9% Δk) in the critical experiments analyzed in Ref. 5. Based upon extrapolation of the trend analysis, AMPX-KENO calculations of the Quad Cities rack would be expected to overpredict k_{∞} by an estimated 3.1% Δk, including allowance for water-gap thickness. Statistically combining the standard deviation of the regression analysis[5] (±0.0027, 1σ) and a typical standard deviation of the KENO variation of the mean (±0.005, 1σ), the maximum uncertainty would be ±0.0116, including a one-sided tolerance factor[6] of 2.03 (95% probability at a 95% confidence level) for an assumed 60 generations in a KENO calculation. Thus, to the extent extrapolation of the linear regression analysis is valid, the AMPX-KENO calculation of the Quad Cities rack will be

high (overprediction) by 0.031 ± 0.012 Δk, or a minimum overprediction of 0.019 Δk including calculational uncertainty. Although extrapolation of the regression trend much beyond the range of the measurements may be questionable, the analysis does indicate that AMPX-KENO calculations would be expected to overpredict k_{eff} when strong boron absorbers are present. No credit is taken for the expected overprediction other than to indicate an additional level of conservatism in the criticality analysis of the Quad Cities spent fuel storage rack.

4.2.4 Reference Fuel Storage Cell

The nominal spent fuel storage cell model used in the criticality analyses is shown in Fig. 4.1. The rack is composed of Boraflex absorber material sandwiched between two 0.075-inch stainless-steel plates. The fuel assemblies are centrally located in each storage cell on a nominal lattice spacing of 6.22 inches. For two-dimensional X-Y analysis, a zero current (reflecting) boundary condition was applied in the axial direction and at the centerline through the Boraflex absorber on all four sides of the cell, effectively creating an infinite array of storage cells. The Boraflex absorber has a nominal thickness of 0.070 inches and a nominal B-10 areal density of 0.01728 grams B-10 per cm^2.

4.3 Reference Subcriticality and Mechanical Tolerance Variations

4.3.1 Nominal Case (8 x 8 Fuel Assembly of 3.2 wt% U-235)

Under normal conditions, with nominal dimensions, the calculated k_{∞} is 0.9155 ± 0.0036 (1σ with 140 generations). For a one-sided tolerance factor of 1.879, corresponding to 95% probability at a 95% confidence limit with 140 generations, the maximum deviation of k_{∞} is ±0.0067.

4.3.2 Alternative Fuel Assemblies

The alternative 8 x 8 fuel assembly of 2.62 wt% U-235 enrichment will have an appreciably lower reactivity than the reference 3.2% enriched assembly, because of the lower enrichment. For the 7 x 7 assembly at an assumed enrichment of 2.8 wt% U-235, AMPX-KENO calculations with nominal dimensions yielded a k_{eff} of 0.890 ± 0.005, which is substantially less than that of the reference 8 x 8 fuel assembly. For the enrichments indicated in Table 4-1, the reactivity would be even lower. Thus, the reference 8 x 8 assembly, with 3.2% U-235 enrichment, is the limiting case.

4.3.3 Boron Loading Variation

The Boraflex absorber plate is nominally 0.070 inches thick with a B-10 areal density of 0.01728 g/cm^2. Manufacturing tolerance limits are ±10% in both thickness and boron content. This assures that, at any point where the minimum boron loading (0.01555 g B-10/cm^2) and minimum Boraflex thickness (0.063 inch) may coincide, the boron areal density will not be less than 0.014 g B-10/cm^2.

Calculations were made of k_{∞} with variations in Boraflex absorber loading and thickness. Results of these calculations, given in Fig. 4.4, indicate that the k_{∞} can be described by the following

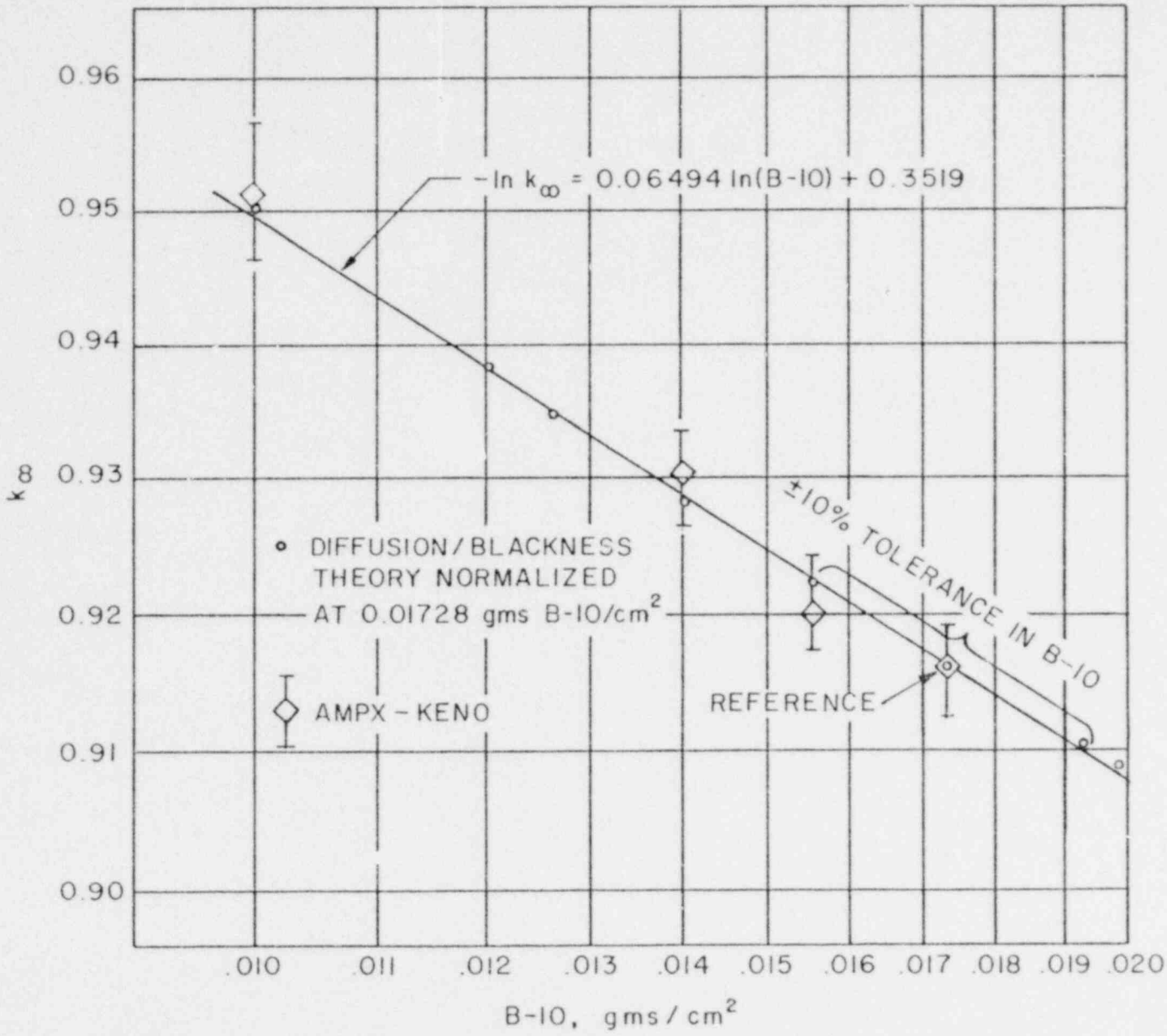

Fig. 4.4 Log-log plot of calculated k_∞ versus B-10 loading.

regression fit (least squares) to the data over the range of B-10 loading from 0.010 to ∿0.020 g/cm^2.

$$-\ln k_{\infty} = 0.06494 \ln (\text{B-10, g/cm}^2) + 0.3519$$

Within the precision of the calculations, this relationship indicates that the 10% tolerance limit on either boron content or Boraflex thickness results in the same incremental reactivity change of ±0.0063 Δk. The trend calculated both by AMPX-KENO and by diffusion/blackness theory is the same within the analytical uncertainty.

4.3.4 Storage Cell Lattice Pitch Variation

The design storage cell lattice spacing between fuel assemblies is 6.220 inches. For manufacturing tolerances of +0.125 or -0.000 inches, increasing the lattice pitch from the minimum 6.220 inches to 6.345 inches (maximum tolerance) reduces reactivity by 0.0113 ± 0.006 Δk, as calculated by AMPX-KENO or by 0.0094 Δk calculated by diffusion/blackness theory. Thus, the nominal case exhibits the largest k_{eff} and the effect on reactivity of a lattice pitch increase is negative. A larger increase in lattice pitch produces an even larger negative effect. Results of calculations at several lattice spacings and boron loadings are shown in Fig. 4.5 in terms of the overall fuel region volume fraction in the spent fuel storage cell (0.6775 for the nominal design).

4.3.5 Stainless Steel Thickness Variations

The nominal stainless-steel thickness is 0.075 inches. The reactivity effect of the expected stainless-steel thickness tolerance variation (±0.002 inches) was calculated to be ±0.0005 Δk by diffusion/blackness theory, since the reactivity increment is too small to be calculated by AMPX-KENO.

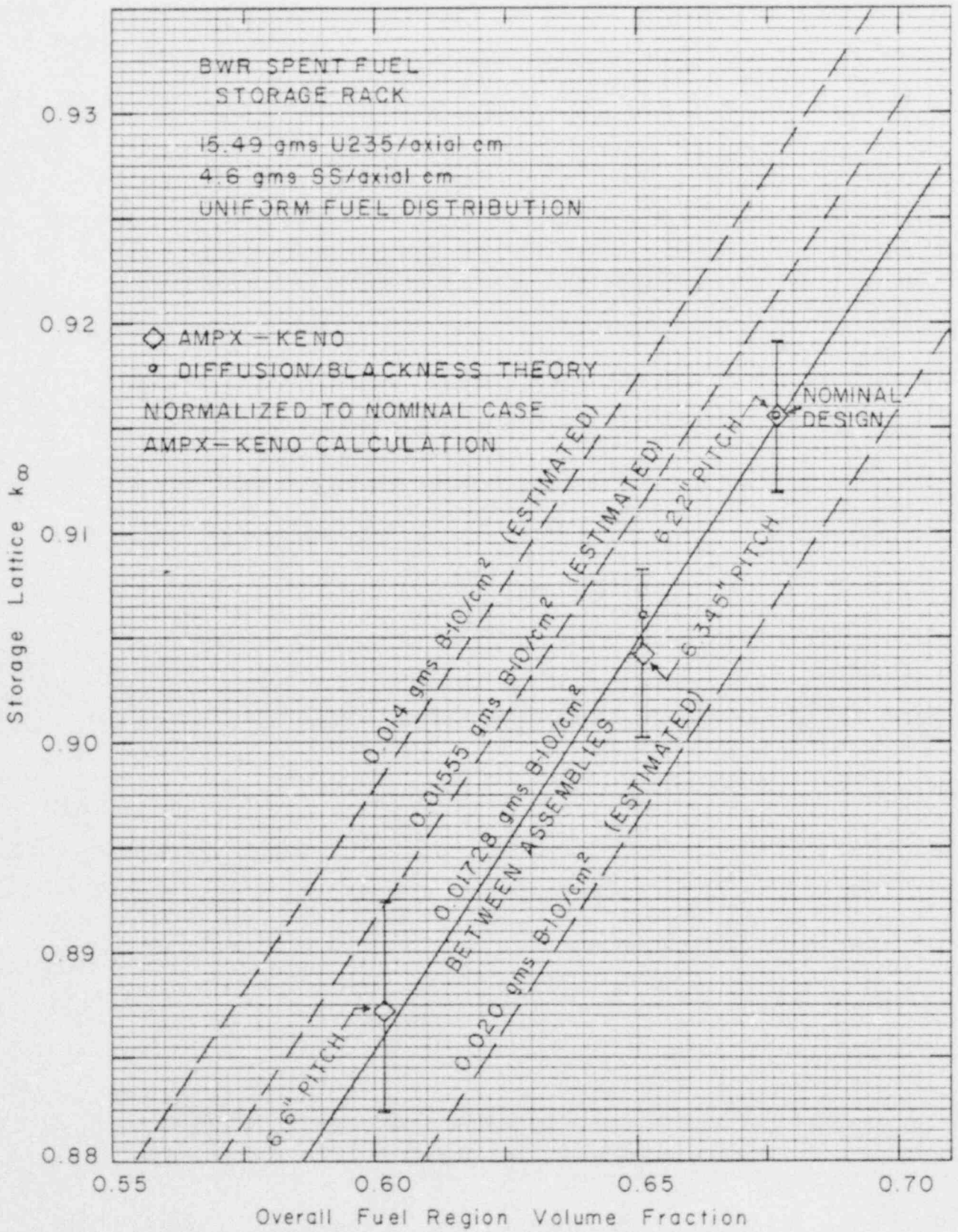

Fig. 4.5 Reactivity effect of lattice spacing and boron loading.

4.3.6 Fuel Enrichment and Density Variation

The design basis enrichment, 3.2 wt% U-235 or 15.49 grams U-235 per axial centimeter in each fuel assembly, defines the fuel of highest anticipated reactivity. Reductions in U-235 enrichment would result in reduced reactivity. Calculations of the sensitivity to small enrichment variations by diffusion/blackness theory yielded an average coefficient of 0.0075 Δk per 0.1 wt% U-235 in the range from 3.1 to 3.3 wt % U-235.

Calculations made with the UO_2 fuel density reduced from the maximum of 10.41 g/cm^3 to 10.25 g/cm^3 indicate that the storage rack k_∞ is reduced by 0.0002 Δk (diffusion/blackness theory). Thus, in the expected range of UO_2 densities, the reactivity effect is negligible.

4.3.7 Boraflex Width Tolerance Variation

The calculational model (Fig. 4.1) uses a Boraflex blade width of 5.86 inches. This is conservative since in the final design of the storage cell, the minimum Boraflex absorber width is nominally 5.91 inches, including tolerances. The calculational model thus results in the highest reactivity (0.9155 ± 0.0036), and the greater width of the actual absorber would further decrease reactivity.

4.3.8 Effect of Zirconium Fuel Channel

Elimination of the zirconium fuel channel results in a small decrease in reactivity (-0.0035 Δk) as calculated by diffusion/blackness theory. More significant is a small positive reactivity effect resulting from bulging of the zirconium channel, which moves the channel wall outward toward the Boraflex absorber. For the maximum expected bulging (to 5.925 inches outside dimension) uniformly throughout the assembly, an incremental reactivity of +0.0039 Δk would result. as calculated by diffusion/blackness

theory using the approximate geometric model for the flow channel indicated by the dotted lines in Fig. 4.1. Since actual bulging of the flow channel would not be the maximum everywhere in all assemblies, the reactivity effect can be statistically combined with the reactivity effect of other mechanical deviations.

Fuel assembly bowing yields a negative reactivity effect and is treated under abnormal conditions (Section 4.4 below).

4.3.8 Summary of Statistical Variations

Calculated reactivity increments from mechanical and fabrication tolerances are summarized in Table 4-2.

Table 4-2 CALCULATED STATISTICAL VARIATIONS IN REACTIVITY (MECHANICAL)

Case	Tolerance	Incremental Reactivity, Δk
Boron concentration	±10%	∓0.0063
Boraflex thickness	±10%	∓0.0063
Lattice pitch	$^{+0.125}_{-0.000}$ inch	Zero to negative
SS tolerance	±0.002 inch	±0.0005
Channel bulge	0.49 inch max	+0.0039
Fuel enrichment and density	*	Zero to negative
Boraflex width	**	Zero to negative
Statistical average (Root-mean-square of positive increment)		±0.0097

---

* Design basis enrichment of 3.2% U-235 by weight is the upper limit.

** Boraflex width used is conservatively less than the minimum width expected including tolerances.

4.4 Abnormal and Accident Conditions

Although credit is permitted for absorption by other absorbers under abnormal conditions, the following evaluations were made without any additional absorber material in the spent fuel storage pool. To the extent any additional absorbers may be present in the realistic case, the following analyses are even more conservative.

4.4.1 Fuel Assembly Positioning in Storage Rack

The fuel assembly is normally located in the center of the storage rack cell with bottom fittings that mechanically prevent lateral movement of the fuel assemblies. Nevertheless, calculations were made with adjacent fuel assemblies (each assumed to be located on one side of its cell with the zirconium fuel channel touching the SS-Boraflex plate) creating an infinite series of two-assembly clusters separated only by the SS-Boraflex plate. For this case, the calculated reactivity was slightly less than the nominal design case (by 0.0011 Δk). Calculations were also made with the fuel assembly moved into the corner of the storage rack cell (four-assembly cluster at closest approach), resulting in an even larger negative reactivity effect (calculated decrease in k_{∞} of $\sim$0.01). With the zirconium fuel channel removed, the reactivity effect of off-set fuel assemblies is even more negative. Thus, the nominal case with the fuel assembly positioned in the center of the storage rack cell, yields the maximum reactivity.

4.4.2 Effect of Zirconium Fuel Channel Distortion

Consequences of bulging of the zirconium fuel channel have been treated as a statistical deviation in Section 4.3.7 above. Bowing of the zirconium channel (including fuel rods, see Fig. 4.2) results in a negative reactivity effect analagous to that of positioning the fuel assembly toward one side of the storage cell

as described in Section 4.4.1 above. Thus, bowing will result in a reduction in reactivity.

4.4.3 Temperature and Water Density Effects

Decreasing temperature from the nominal 68°F to 39°F (maximum water density) is calculated to increase reactivity by 0.0007 Δk, as indicated in Table 4-3 (reactivity effects calculated by diffusion/blackness theory). Increasing the water temperature or introducing voids (to simulate boiling) decreases reactivity, as shown in the table.

Table 4-3 EFFECT OF TEMPERATURE AND VOID ON CALCULATED REACTIVITY OF STORAGE RACK

Case	Δk_{∞}	Comment
39°F	+0.0007	Maximum water density
68°F	0	Reference
104°F	-0.004	$\rho(H_2O) = 0.992$
176°F	-0.013	$\rho(H_2O) = 0.972$
212°F	-0.020	$\rho(H_2O) = 0.958$
212°F with 50% void	-0.175	Simulates boiling

4.4.4 Abnormal Positioning of Fuel Assembly Outside Storage Rack

Since the storage rack criticality calculations were made assuming an infinite array of storage cells, positioning a fuel assembly outside and adjacent to the actual rack cannot add reactivity; such positioning would result in a k_{eff} that is lower than the k_{∞} calculated for the infinite array. This has been confirmed by two-dimensional PDQ analysis of finite racks with a new fuel element positioned outside and adjacent to the rack.

4.4.5 Missing Absorber Plate

Should a Boraflex absorber plate be missing from between fuel assemblies — i.e., postulated to be lost by an undefined accident — the reactivity will be slightly higher than the reference case. Calculations performed in two dimensions (PDQ7) indicate the largest reactivity increment is less than +0.0031 Δk due to the loss of a single plate. Because of mesh size limitations in PDQ7, symmetry considerations (with reflective boundary conditions) effectively resulted in the loss of an absorber plate from one side of every 15 storage cells. Thus, the calculated incremental reactivity addition due to the loss of an absorber plate should be conservative.

4.4.6 Dropped Fuel Assembly Accident

A postulated fuel assembly drop into and to the bottom of a storage rack cell results in a configuration that is that of the nominal cell configuration; therefore, a drop will not result in a reactivity greater than that of the nominal design case.

To investigate the possible reactivity effects of other postulated drop accidents, calculations were made for unpoisoned assemblies separated only by water. Figure 4.6 shows the results of these calculations. From these data, the reactivity (k_{∞}) will be less than 0.95 for any spacing greater than ~8 inches. For a straight drop on top of the rack, an inclined drop or a fuel assembly lying horizontally on the top of the rack, the minimum separation distance is ~9 inches. Maximum expected deformation under seismic or accident conditions (see Sections 6 and 7) will not reduce the minimum spacing to less than 8 inches. In addition, the upper 6 inches of fuel is natural uranium oxide, which affords a further effective separation from the higher-enriched active fuel in the storage racks. Finally, a three-dimensional PDQ analysis, with a new fuel element immediately above the active fuel in the

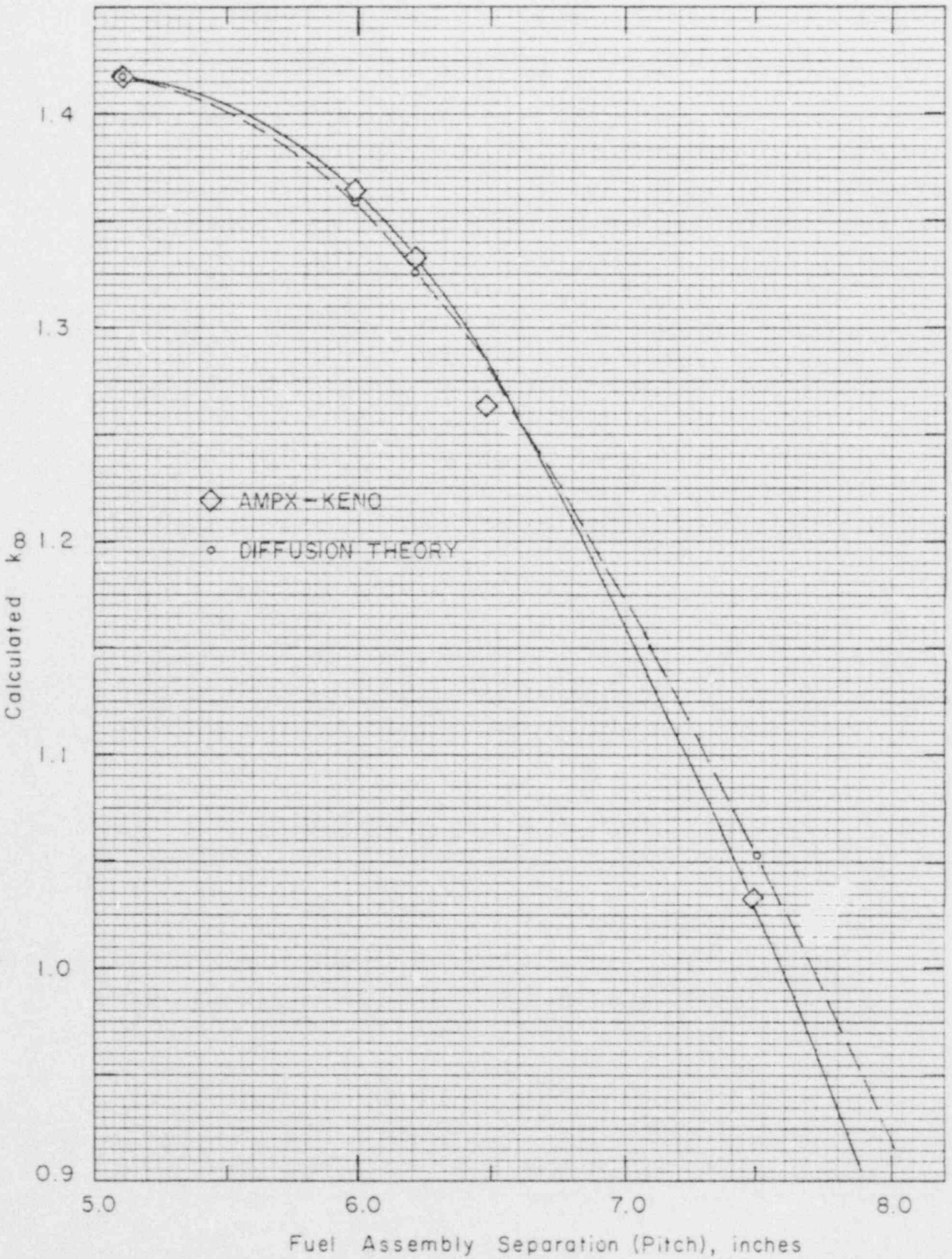

Fig. 4.6 Reactivity effect of separation between fuel assemblies (unpoisoned).

storage rack (neglecting structural material) confirms that the reactivity is less than that of the design basis infinite array.

Fuel assembly drop accidents will not result in an increase in reactivity above that calculated for the infinite nominal design storage rack.

4.4.7 Fuel Rack Lateral Movement

Normally, the individual racks in the spent fuel pool are separated by a water-gap of 1 to 2 inches. For finite fuel racks, this separation would reduce the actual maximum reactivity of the racks. Should lateral motion of a fuel rack occur, for whatever reason, closing the gap between racks, the reactivity would, in the limit, only approach the limiting reactivity of the reference infinite array.

4.5 Summary

The criticality analyses of the spent fuel storage rack under normal and abnormal conditions are summarized in Table 4-4.

Table 4-4 SUMMARY OF CRITICALITY CALCULATIONS

Case		k_∞ or Δk_∞	Comment
Normal Conditions			
k_∞, reference		0.9155	Section 4.3.1
Calculational bias		+0.0036	Includes gap correction
Uncertainties			
Bias	±0.0123		Section 4.2.3
Calculational	±0.0067		Section 4.3.1
Mechanical	±0.0097		Section 4.3.8, Table 4-2
		±0.0170	Statistical combination
Total		0.9191 ± 0.0170	
Maximum k_∞		0.9361	
Abnormal and Accident Conditions			
Decreased temperature		+0.0007	Maximum water density
Increased temperature or void		negative	
Fuel element positioning		negative	
Fuel channel bowing		negative	
Lost/missing absorber plate		+0.0031	Conservative
Fuel handling accident		negligible	
Lateral rack movement		negligible	

Thus, a k_∞ of 0.936 is conservatively estimated to be the maximum k_∞ under the worst combination of calculational and mechanical uncertainties (normal conditions), with a 95% probability at a

95% confidence level. Under the worst combination of abnormal and accident conditions, the maximum k_{∞} could be as much as 0.940.

Removal of the zirconium fuel channel from all assemblies would reduce the maximum k_{∞} to 0.933 (normal conditions). If the trend toward overprediction with boron worth (Section 4.2.3.3) is valid, the maximum expected k_{∞} under normal conditions would be 0.905.

REFERENCES

1. Green, Lucious, Petrie, Ford, White, Wright, PSR-63/AMPX-1 (code package), AMPX Modular Code System for Generating Coupled Multigroup Neutron-Gamma Libraries From ENDF/B, ORNL-TM-3706, Oak Ridge National Laboratory, March 1976.

2. L. M. Petrie and N. F. Cross, KENO-IV, An Improved Monte Carlo Criticality Program, ORNL-4938, Oak Ridge National Laboratory, November 1975.

3. S. R. Bierman et al., Critical Separation Between Subcritical Clusters of 4.29 wt% U^{235} Enriched UO_2 Rods in Water with Fixed Neutron Poisons, NUREG/CR-0073, Battelle Pacific Northwest Laboratoryies, May 1978, with errata sheet issued by the USNRC August 14, 1979.

4. M. N. Baldwin et al., Critical Experiments Supporting Close Proximity Water Storage of Power Reactor Fuel, BAW-1484-7, The Babcock & Wilcox Company, July 1979.

5. S. E. Turner and M. K. Gurley, Benchmark Calculations for Spent Fuel Storage Racks, Report SSA-127, Southern Science Applications, Inc., July 1980.

6. M. G. Natrella, Experimental Statistics, National Bureau of Standards, Handbook 91, August 1963.

5. HYDRO-THERMAL CONSIDERATIONS

A central objective in the design of the high density fuel rack is to ensure adequate cooling of the fuel assembly cladding. In the following, a brief synopsis of the design basis, method of analysis and computed results is given.

5.1 Heat Generation Calculations:

Later

5.2 Analysis of Pool Thermal-Hydraulics

In order to determine an upper bound on the maximum fuel cladding temperature, a series of conservative assumptions are made. The most important assumptions are listed below:

a. As stated above, the fuel pool will contain spent fuel with varying "time-after-shut-down" t_s. Since the heat emission falls off rapidly with increasing t_s, it is obviously conservative to assume that all fuel assemblies are fresh (t_s = 100 hours), and they all have had four years of operating time in the Reactor (Ref. 1). The heat emission rate of each fuel assembly is assumed to be equal, and it can be computed from Ref. (2).

b. As shown in Figures 2.1 and 2.2, the modules occupy an irregular floor space in the pool. For purposes of the hydrothermal analysis, a circle circumscribing the actual rack floor space is drawn. It is further assumed that the cylinder with this circle as its base is packed with fuel assemblies at the nominal pitch of 6.22". (Figure 5.1).

c. The downcomer space around the rack module group varies, as shown in Figure 5.1. The minimum downcomer gap (7½") available in the pool is assumed to be the total gap available around the idealized cylindrical rack; thus, the maximum resistance to downward flow is incorporated into the analysis.

d. No downcomer flow is assumed to exist between the rack modules.

In this manner, a conservative idealized model for the rack assemblage is devised. The water flow is axisymmetric about the vertical axis of the circular rack assemblage, and thus, the flow is two dimensional (axisymmetric three dimensional). The governing equation to characterize the flow field in the pool can now be written. It is shown in Ref. (4) that the resulting integral equation can be solved for the lower plenum velocity field (in the radial direction) and axial

velocity (in-cell velocity field), by using the method of collocation. It should be added here that the hydrodynamic loss coefficients which enter into the formulation of the integral equation are also taken from well recognized sources in the literature; and wherever discrepancies in reported values exist, the conservative values are consistently used.

After the axial velocity field is evaluated, it is a straight-forward matter to compute the fuel assembly cladding temperature. The knowledge of the overall flow field enables pinpointing the storage location with the minimum axial flow (i.e: maximum water outlet temperature). This is called the most "choked" location. It is recognized that these storage locations, where rack module supports are located, have some additional hydraulic resistance not encountered in other cells. In order to find an upper bound on the temperature in such a cell, it is assumed that it is located at the most "choked" location. Knowing the global plenum velocity field, the revised axial flow through this choked cell can be calculated by solving the bernoulli's equation for the flow circuit through this cell. Thus, an absolute upper bound on the water exit temperature and maximum fuel cladding temperature is obtained. It is believed that in view of the preceding assumption, the temperatures calculated in this manner over-estimate the temperature rise that will actually be obtained in the pool.

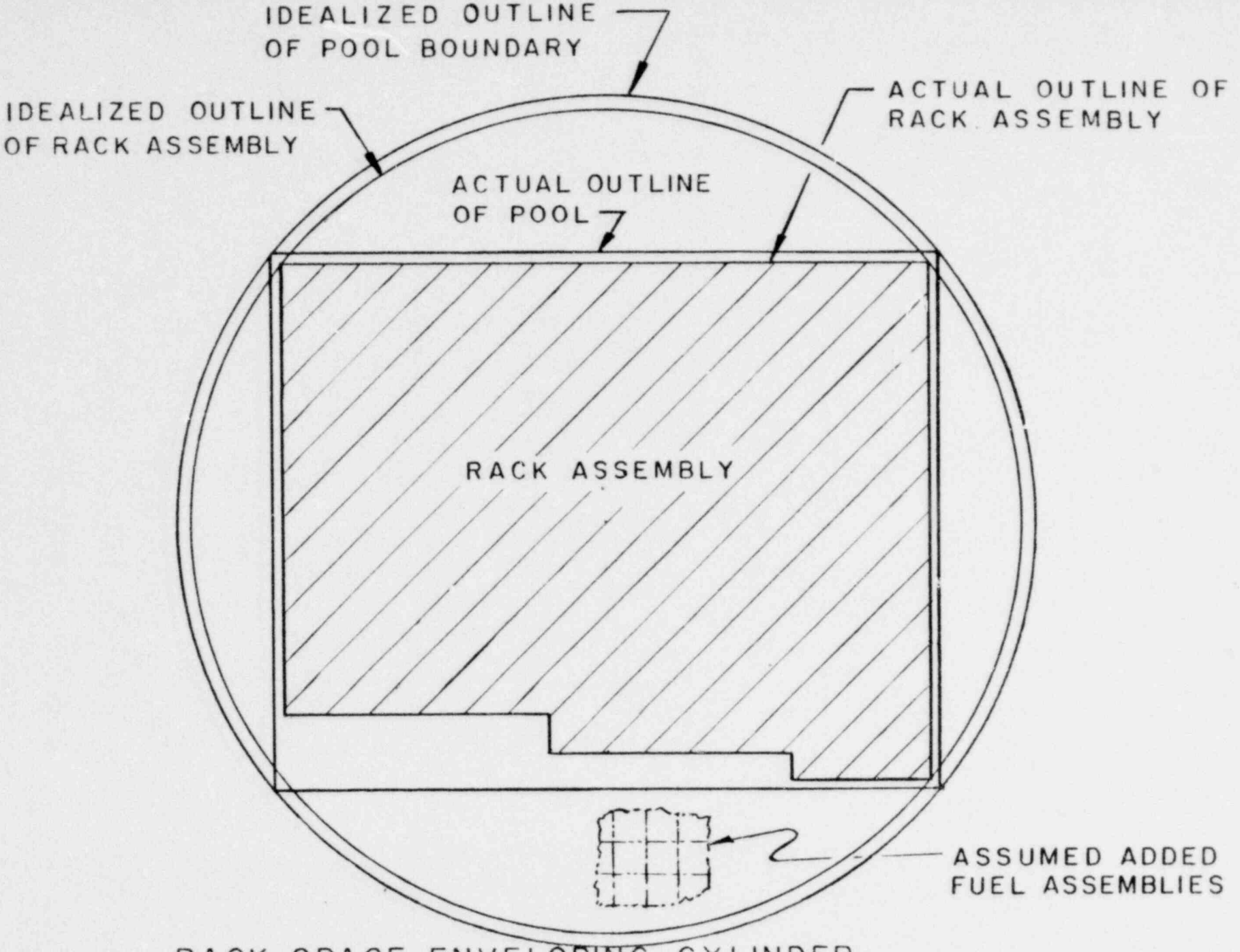

FIG. 5.1 RACK SPACE ENVELOPING CYLINDER
(QUAD-CITIES STATION UNIT 1 & 2)

REFERENCES TO SECTION 5

1. FSAR, Quad-Cities, Section 10, Auxiliary and Emergency Systems.

2. U.S. Regulatory Commission, Standard Review Plan, Branch Technical Position. APCSB 9-2 Rev. 1, Nov. 1975.

3. "A Method for Hydro-Thermal Analysis of High Density Fuel Racks", Oat Standard Document #20, Rev. 1, (1980).

6. SEISMIC ANALYSIS

6.1 Analysis Outline

The spent fuel storage racks are seismic category I equipment. Thus, in accordance with Ref. (1), they are required to remain functional during and after an SSE (Safe Shutdown Earthquake). As noted previosly, these racks are neither anchored to the pool floor, nor are they attached to the side walls. The individual rack modules are not interconnected. Furthermore, a particular rack may be completely loaded with fuel assemblies (which corresponds to greatest rack inertia), or it may be partially loaded so as to produce maximum geometric eccentricity in the structure. The coefficient of friction, μ, between the supports and pool floor is another indeterminate factor. According to Rabinowicz [2], the results of 199 tests performed on austenitic stainless plates submerged in water show a mean value of μ to be .503 with a standard deviation of 0.125. The upper and lower bounds ($\mu \pm 2\sigma$) are thus 0.753 and .253, respectively. Two separate analyses are performed for this rack assembly with values of μ equal to 0.2 (lower limit), and 0.8, respectively. In summary, the following six separate analyses are performed:

1. Fully loaded rack (all storage locations occupied);
   $\mu = 0.8$ (μ = coefficient of friction)
2. Fully loaded rack, $\mu = 0.2$
3. Half loaded rack to produce maximum geometric asymmetry about the major dimension of the rectangular rack
   $\mu = 0.8$
4. Half loaded rack to produce maximum geometric asymmetry about the major dimension of the rectangular rack
   $\mu = 0.2$
5. Half loaded rack to produce maximum loading asymmetry about a diagonal
   $\mu = 0.8$
6. Half loaded rack to produce maximum loading asymmetry about a diagonal
   $\mu = 0.2$

The method of analysis employed is the Time History method. The ground acceleration coincidently in three directions is specified by the owner of the power plant.

The object of the seismic analysis is to determine the structural response (stresses, deformation, rigid body motion, etc.) due to simultaneous application of the three orthogonal excitations. Thus, recourse to approximate statistical summation techniques such as SRSS method (Ref. 3) is avoided and the dependability of computed results is ensured.

The siesmic analysis is performed in four steps; namely

(i) Development of non-linear dynamic model consisting of beam, gaps, spring, damper and inertia coupling elements;

(ii) Derivation and computation of element stiffnesses using a sophisticated elastostatic model;

(iii) Layout the equations of motion, decouple these equations and solve them using the "component element time integration" procedure (Ref. 4). Determine nodal forces.

(iv) Compute the detailed stress field in rack structure using the detailed elastostatic model from the nodal forces calculated in Step III above. Determine if the stress and displacement limits (given in Section 6.5) are satisfied.

A brief description of the dynamic model now follows.

6.2 Fuel Rack - Fuel Assembly Model

6.2.1 Assumptions

a. The fuel rack metal structure is represented by five lumped masses connected by appropriate elastic springs. (Refer to Figure 6.1).

b. The fuel assemblies are represented by five lumped masses located, relative to the rack, in a manner which simulates either full or partially filled conditions.

c. The fuel rack base is considered as a rigid body supported at four points.

d. The rack base supports may slide or lift off the pool floor.

e. The pool floor is assumed to have a known ground acceleration in three orthogonal directions.

f. Fluid coupling between rack and assemblies, and between rack and adjacent racks is simulated by introducing appropriate inertial coupling into the system kinetic energy.

g. Potential impacts between rack and assemblies is accounted for by appropriate spring gap connectors between masses involved.

h. Fluid damping between rack and assemblies, and between rack and adjacent rack is simulated by inclusion of appropriate equivalent linear damping.

i. The supports are modeled as rigid beams for dynamic analysis. The bottom of the support legs is attached to a frictional spring as described in Section 6.2.2. The elastic properties of the support beams are derived and used in the final computations to determine support leg stresses.

j. The effect of sloshing is shown to be negligible and is hence neglected. It is to be noted that the top of the rack is over 20' below the free water surface.

6.2.2 Model Description

The absolute degrees of freedom associated with each of the mass locations i, i* is as follows (Figure 6.1).

LOCATION (NODE)	DISPLACEMENT u_x	u_y	u_z	ROTATION θ_x	θ_y	θ_z
1	P_1	P_2	P_3	q_4	q_5	q_6
1*	Point is assumed fixed to base at XB,YB,Z=0					
2	P_7	P_9		q_{11}	q_{12}	
2*	P_8	P_{10}				
3	P_{13}	P_{15}		q_{17}	q_{18}	
3*	P_{14}	P_{16}				
4	P_{19}	P_{21}		q_{23}	q_{24}	
4*	P_{20}	P_{22}				
5	P_{25}	P_{27}	P_{32}	q_{29}	q_{30}	q_{31}
5*	P_{26}	P_{28}				

Thus, there are 32 degrees of freedom in the system.

Note that elastic motion of the rack in extension is represented by generalized coordinates P_3 and P_{32}. This is due to the relatively high axial rigidity of the rack. Torsional motion of the rack relative to its base is governed by q_{31}.

A schematic description of the rack supports is given in Figure 6.2. The members joining nodes 1 to 2, 2 to 3, etc., are beam elements with deflection due to bending and shear capability (Ref. 4, pp 156-161). The elements of the stiffness matrix of these beam elements are readily computed if the effective flexure

modulus, torsion modulus, etc. for the rack structure are known. These coefficients follow from the elastostatic model as described later. The node points i^* (i = 1,2 ... 5) denote the cumulative mass for all the fuel assemblies distributed at 5 elevations. Referring to G.E. specification (Ref. 5), the bending and torsional stiffnesses of the fuel assembly (channeled or unchanneled) are several orders of magnitude smaller than the rack beam elements. Hence, it is reasonable to neglect the spring elements joining these lumped masses. In order to demonstrate that fuel assembly structural springs can be disregarded to produce conservative results, the case (refer to Section 6.1) which yields maximum rack primary stress is also run with beam springs connecting fuel assembly lumped masses. The results are available in Ref. (7). The nodes i^* are located at $X = X_B$, $Y = Y_B$ in the global coordinate system shown in Figure 6.1. The coordinates (X_B, Y_B) are determined by the center-of-mass of the set of fuel assemblies. For a completely loaded rack $X_B = Y_B = 0$.

6.2.3 Fluid Coupling

An effect of some significance requiring careful modeling is the so-called "fluid coupling effect". If one body of mass m_1 vibrates adjacent to another body (mass m_2), and both bodies are submerged in a frictionless fluid medium, then the Newton's equation of motion for the two bodies have the form

$$(m_1 + M_{11})\ddot{X}_1 - M_{12}\ddot{X}_2 = \text{applied forces on mass } m_1 \quad (6.1)$$

$$-M_{21}\ddot{X}_1 + (m_2 + M_{22})\ddot{X}_2 = \text{applied forces on mass } M_2$$

M_{11}, M_{12}, M_{21} and M_{22} are fluid coupling coefficients which depend on the shapes of the two bodies, their relative disposition; etc. Fritz (5) gives data for M_{ij} for various body shape and arrangements. It is to

be noted that the form of Eq. (6.1) indicates that effect of the fluid is to add a certain amount of mass to the body (M_{11} to body 1), and an external force which is proportional to the acceleration of the adjacent body (mass m_2). Thus, the acceleration of one body affects the force field on another. This force is a strong function of the inter-body gap, reaching large values for very small gaps. This inertial coupling is called fluid coupling. It has an important effect in rack dynamics. The lateral motion of a fuel assembly inside the storage location will encounter this effect. So will the motion of a rack adjacent to another rack. These effects are included in the equations of motion as described in detail in Reference (6). The fluid coupling is between nodes i and i^* (i = 2, 3 ... 5) in Figure 6.1. Furthermore, nodal masses i are coupled to the reference frame through inertial coupling coefficients.

Finally, virtual mass is included in vertical direction vibration equations of the rack; and virtual inertia is added to the governing equations corresponding to rotational degrees of freedom, such as q_4, q_5, q_6, q_{11}, etc.

6.2.4 Damping

In reality, damping to the rack motion arises from material hysteresis (material damping), relative inter-component motion in structures (structural damping), and fluid drag effects (fluid damping). (Ref. 17)

Only fluid damping is included in the analysis. The fluid damping acts on the i^* nodal masses, as well as on i nodal masses. The equivalent values of linear dampers for various types of motions are derived in Ref. (7). An analysis of rack stresses in the absence of fluid damping is also performed to obtain an understanding of the contribution of damping in abating stresses and displacements.

6.2.5 Impact

The fuel assembly nodes i^* will impace the corresponding structural mass node i. To simulate this impact, 4 impact springs around each fuel assembly node are provided (Figure 6.3). The fluid dampers are also provided in parallel to the springs. The spring constant of the springs is equal to the local stiffness of the vertical panel computed by evaluating the deflection of a 6" diameter circular plate (.075") uniformly loaded and built in around the edge. The spring constant calculated in this manner should provide an upper bound on the local stiffness of the structure.

A brief description of the elastostatic model now follows.

6.3 Stress Analysis

6.3.1 Stiffness Characteristics

The fuel rack is a multi-cell, folded-plate structure which has what is colloquially called an "egg-crate" configuration. This type of construction is very similar to the so-called "stressed-skin" construction of ribs spars and cover plates which are widely used in aircraft construction. Techniques developed in the field of aircraft structural analysis are utilized herein to find the stresses and deformations in such structures. These methods have been thoroughly tested and their reliability has been documented in a number of well-known publications (e.g. Ref. 8 thru 12).

Figure 6.4 shows two cross-sections of the fuel rack which is modeled as a rectangular network of plates interconnected along nodal lines shown as points in Fig. 1-A. An arbitrary load with components Fx^i, Fy^i, Fz^i acts as an arbitrary elevation on one of the nodal lines. We find the displacements and stresses due to such a typical load according to the stressed skin model as follows:

The torsional deformations are solved for by using the classical theory of torsion for multi-celled, thin-walled cross-sections (Ref. 13).

The bending deofmration is found by using the theory of shear flow (Ref. 12) wherein all axial stresses are carried by the effective flanges (or stringers) formed by the intersections of the plates and all transverse shears are carried by the plates modeled as shear panels.

From a knowledge of the shear flows, the bending and torsional deformations, it is possible to provide a set of influence functions or the following section properties for the fuel rack as a whole:

$(EI)_{eq}$ = Bending rigidity (in two places)

$(GJ)_{eq}$ = Torsional rigidity

$(AE)_{eq}$ = Extensional rigidity

k_s = Shear deformation coefficient

Such properties are used for the dynamic analysis of seismic loads. The detailed equations are documented in Ref. (7).

6.3.2 Combined Stresses and Corner Displacements

The cross-sectional properties and the Timoshenko shear correction factor calculated in the previous section are fed into a dynamic analysis of the systme shown in Figure 6.5 with a specified ground motion simulating earthquake loading. From the dynamic analysis, the stress resultants (F_x, F_y, F_z, M_x, M_y, M_z) acting as shown in Figure 6.6 are computed for a large number of times $t = \Delta t$, $2\ \Delta t$ ... etc, at a selected number of cross sections. The displacements (U_x, U_y, U_z) at selected nodal points on the z axis are also provided by the dynamic analysis as well as rotations (θ_x, θ_y, θ_z) of the cross-sections at the nodes.

Figure 6.7 shows a typical sub-division of the structure into elements, nodes and sections. The stresses are calculated at all sections and the displacements at all four corners of the rack are calculated at these elevations.

Since σ varies linearly over the cross-section and achieves its extreme values at one of the four corners of the rack, the shear stresses due to torsional loads (M_z) achieve their extreme values near the middle of each side. The shear stresses due to lateral forces (F_x, F_y) will achieve their extreme values at the center of the cross section or at the

middle of each side (see Ref. 7). Thus, candidates for the most critical point on any section will be the points labelled 1, 2 ... 9 in Figure 6.8. The expression for the combined stress and kinematic displacement for each of these points is written out. Similarly the stresses in the support legs are evaluated.

An Oat proprietary computer program "EGELAST" computes the stresses at the candidate points in each level. It sorts out the most stressed location in space as well as time. The highest stress, and maximum kinematic displacement are thus readily found.

6.4 Time Integration of the Equations of Motion

Having assembled the structural model, the dynamic equations of motion corresponding to each degree of freedom can be written by using Newton's second law of motion; or using Lagrange's equation. For example, the motion of Node 2 in x-direction (governed by the generalized coordinate p_7) is written as follows:

The inertial mass is

$$m_{21} + A_{211} + B_{211}$$

where m_{21} is the mass of node 2 for x-directional motion.

A_{211} is the fluid coupling mass due to interaction with node 2*.

B_{211} is the fluid coupling mass due to interaction of node 2 with the reference frame (interaction between adjacent racks).

Hence Newton's law gives

$$(m_{21} + A_{211} + B_{211}) \ddot{p}_7 + A_{212} \ddot{p}_8 + B_{212} \ddot{u} = Q_2$$

where Q_2 represents all the beam spring and damper forces on node 2, and A_{212} is the cross term fluid coupling effect of node 2*; and B_{212} is the cross term fluid coupling effect of the adjacent racks. $\ddot{u}$ represents the ground acceleration.

Let

$$q_7 = p_7 - u$$

i.e: q_7 is the relative displacement of node 2 in x-direc- with respect to the ground. Substituting in the above equation, and rearranging, we have

$$(m_{21} + A_{211} + B_{211}) \ddot{q}_7 + A_{212} \ddot{q}_8 = Q_2 - (m_{21} + A_{211} + B_{211} + A_{212} + B_{212}) \ddot{u}$$

Similar equation for each one of the 32 degrees of freedom can be written out. The system of equations can be represented in matrix notation as:

$$[M]\{\ddot{q}\} = [Q] + \{G\}$$

where the vector [Q] is a function of nodal displacement and velocities, and {G} depends on the coupling inertias and the ground acceleration.

Pre-multiplying above equation by $[M]^{-1}$ renders the resulting equations uncoupled in mass.

We have:

$$\{\ddot{q}\} = [M]^{-1}\,[Q] + [M]^{-1}\,\{G\}$$

This equation set is mass uncoupled, displacement coupled; and is ideally suited for numerical solution using the central difference scheme. The computer program developed by G.E. and described in Ref. (4) performs this task in an efficient manner. This computer program, named "DYNAHIS" in Oat's computer program library is documented in Ref. (4), and also internally at Oat.

Having determined the internal forces as a function of time, the computer program "EGELAST" computes the detailed stress and displacement field for the rack structure as described in the preceding section.

6.5 Structural Acceptance Criteria

There are two sets of criteria to be satisfied by the rack modules:

(a) Kinematic Criteria: This criterion seeks to ensure that adjacent racks will not impact during SSE (condition E' in Ref. 14), assuming the lower bound value of the pool surface friction coefficient. It is further required that the factors of safety against tilting specified in Ref. (15) are met (1.5 for OBE, 1.1 for SSE).

(b) Stress Limits: The stress limits of the ASME Code.

(1) Criteria: Section III, Sub-Section NF, 1980 Edition with latest Addendum were chosen to be met, since this Code provides the most consistent set of limits for various stress types, and various loading conditions. The following loading cases (taken out of the set specified in Ref. (14) are meaningful.

	SRP Designation	ASME Designation
(i)	D + L	Level A (normal condition)
(ii)	D + L + E	Level B (upset condition)
(iii)	D + L + T_o	No ASME Designation. Primary membrane plus bending stress required to be limited to lesser of 2 S_y† and S_u†
(iv)	D + L + T_o + E	No ASME Designation. Stress limit same as (iii) above
(v)	D + L + T_a + E	No ASME Designation. Stress limit same as above
(vi)	D + L + T_a + E'	Level D (faulted condition)

where

D: Dead weight induced stresses

L: Live load induced stresses

E: O.B.E. (Time history loading)

E': S.S.E.

T_o: Stresses due to assymmetric heat emission from the fuel assemblies

T_a: Thermal stresses due to postulated high energy pipe break

---

†S_y: Yield stress of the material, S_u: ultimate stress

The conditions T_a and T_o cause local thermal stresses to be produced. The worst situation will be obtained when an isolated storage location has a fuel assembly which is generating heat at the maximum postulated rate. The surrounding storage locations are assumed to contain no fuel. Furthermore, the loaded storage location is assumed to have unchanneled fuel. Thus, the heated water makes unobstructed contact with the inside of the storage walls thereby producing maximum possible temperature difference between the adjacent cells. The secondary stresses thus produced are limited to the body of the rack. i.e., the support legs do not experience the secondary (thermal) stresses.

(2) Basic Data: The following data on the physical properties of the rack material are obtained from the ASME Code, Section III, appendices.

TABLE 6.1 PHYSICAL PROPERTY DATA†

Property	Young's Modules E	Yield Strength S_y	Ultimate Strength S_u	Allowable Stress S
Value	28.3×10^6 Psi	25 KSI	71 KSI	17.8 KSI
Reference	Table I-6.0	Table I-2.2	Table I-3.2	Table I-7.2

(3) Stress limits for normal, upset and faulted conditions: The following limits are obtained from NF-3230 in conjunction with Appendix XVII as modified by the USNRC Regulatory Guide 1.124.

(3.1) Normal and upset conditions (level A or level B).

(i) Allowable stress in tension on a net section = $F_t = .6S_y$ or $F_t = (.6)(25000) + 15000$ Psi

F_t is equivalent to primary membrane stresses

†Evaluated at 200°F. This temperature is higher than the pool water bulk temperature under any of the loading conditions under consideration.

(ii) On the gross section, allowable stress in shear is

$$F_v = 0.4\ S_y$$

$$= (0.4)(25000) = 10{,}000\ \text{Psi}$$

(iii) Allowable stress in compression, F_a

$$F_a = \frac{\left[1 - \left(\frac{kl}{r}\right)^2 / 2C_c^2\right] S_y}{\left[\left(\frac{5}{3}\right) + \frac{^3\left(\frac{kl}{r}\right)}{8C_c} - \frac{\left(\frac{kl}{r}\right)^3}{8C_c^3}\right]}$$

where

$\frac{kl}{r}$ = the largest effective slenderness ratio

$$C_c = \left(\frac{2\pi^2 E}{S_y}\right)^{\frac{1}{2}} = 147.81$$

Substituting numbers, we obtain, for both support leg and "egg crate" region:

$F_a = 15000$ Psi

(iv) Maximum bending stress at the outermost fiber due to flexure about <u>one</u> plane of symmetry:

$F_b = .60S_y = 15000$ Psi

(v) Combined flexure and compression:

$$\frac{f_a}{F_a} + \frac{C_{mx}\ f_{bx}}{D_x\ F_{bx}} + \frac{C_{my}\ f_{by}}{D_y\ F_{by}} \leq 1$$

where

f_a: Direct compressive stress in the section

f_{bx}: Maximum flexural stress x-axis

f_{by}: Maximum flexural stress y-axis

$C_{mx} = C_{my} = 0.85$

$D_x = 1 - \frac{f_a}{F'_{ex}}$

$$D_y = 1 - \frac{f_a}{F'_{ey}}$$

where

$$F'_{ex} = \frac{12\pi^2 E}{23\left(\frac{k l_b}{r_b}\right)^2}$$

(vi) Combined flexure and compression (or tension)

$$\frac{f_a}{.6\ S_y} + \frac{f_{bx}}{F_{bx}} + \frac{f_{by}}{F_{by}} \leq 1.0$$

The above requirement should be met for both direct tension or compression case.

(3.2) Faulted Condition:

F-1370 (Section III, Appendix F), states that the limits for the faulted condition are

$1.2\ \left(\frac{S_y}{F_t}\right)$ times the corresponding

limits for normal condition. Thus the multiplication factor is

$$\text{Factor} = (1.2)\left(\frac{25000}{15000}\right) = 2.0$$

(3.3) Thermal Stresses:

There are no stress limits for thermal (self-limiting) stresses in Class 3-NF Structures for linear type supports.

However, the range of primary and secondary stress intensity is required to be limited to 3 S_m in the manner of class 1 components. S_m is the allowable stress intensity of the rack material at the maximum operating temperature.

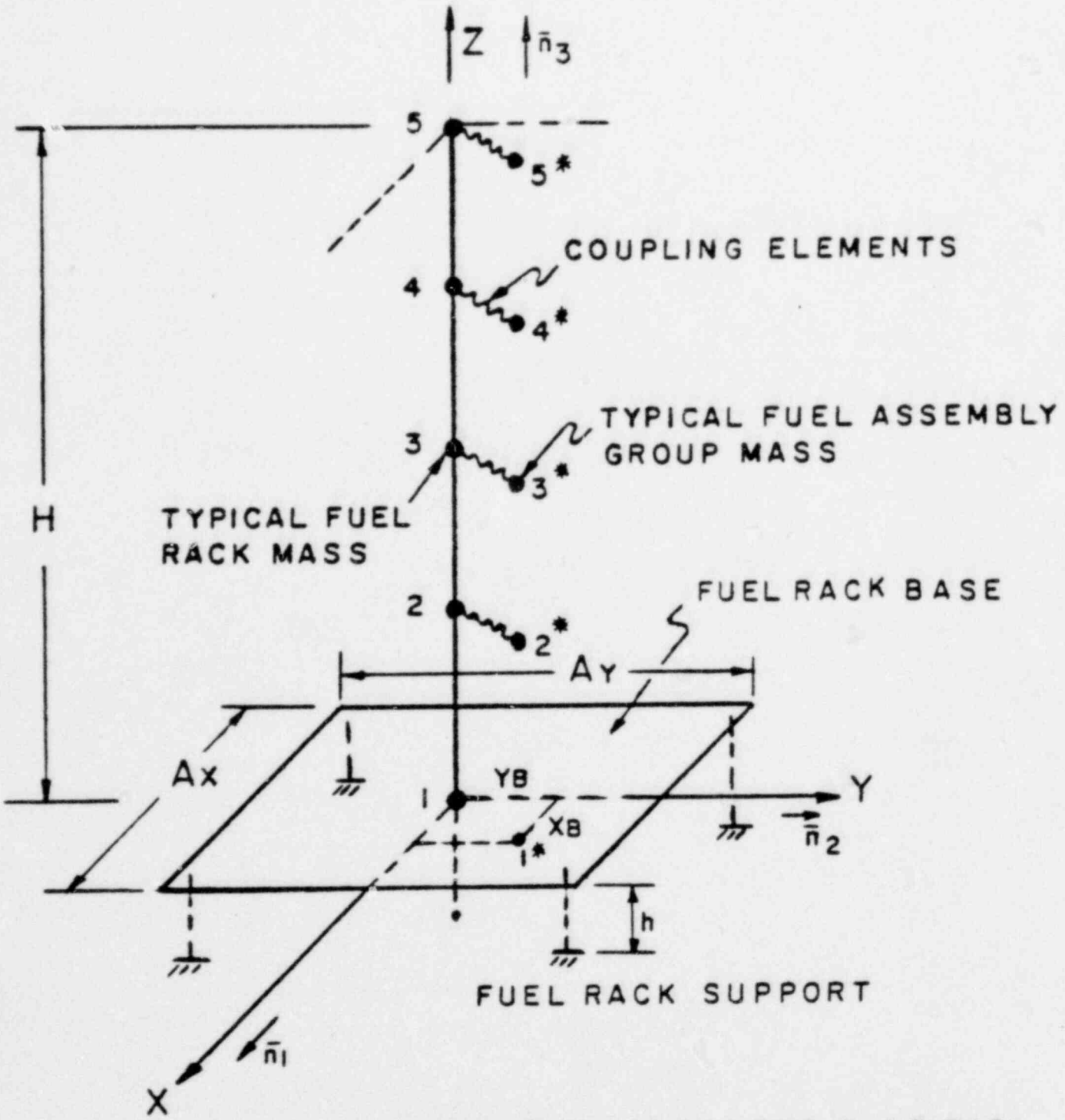

XB, YB - LOCATION OF CENTROID OF FUEL ROD GROUP MASSES - RELATIVE TO CENTER OF FUEL RACK

n_i = UNIT VECTORS

FIG. 6.1 DYNAMIC MODEL

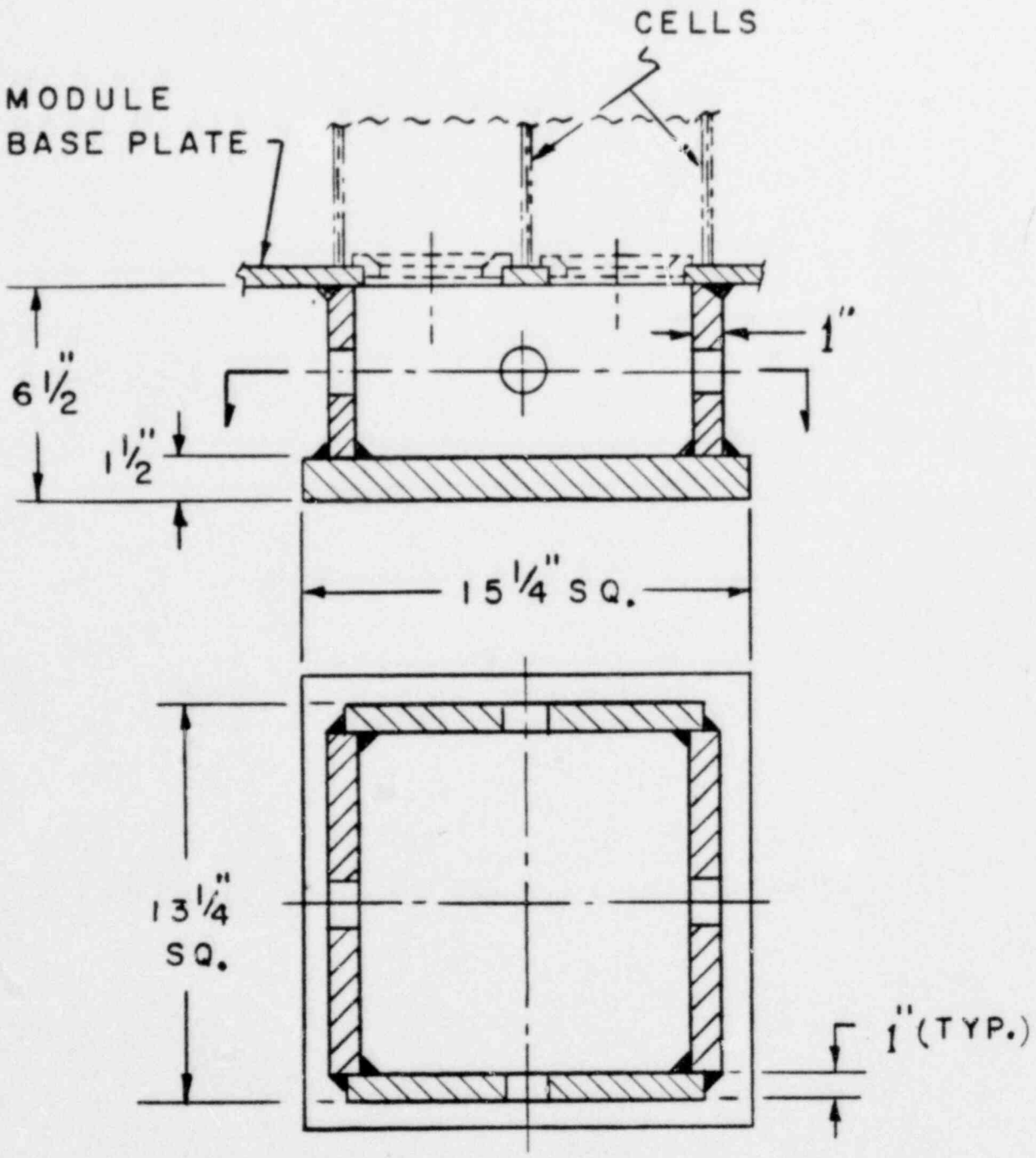

FIG. 6.2 SUPPORT

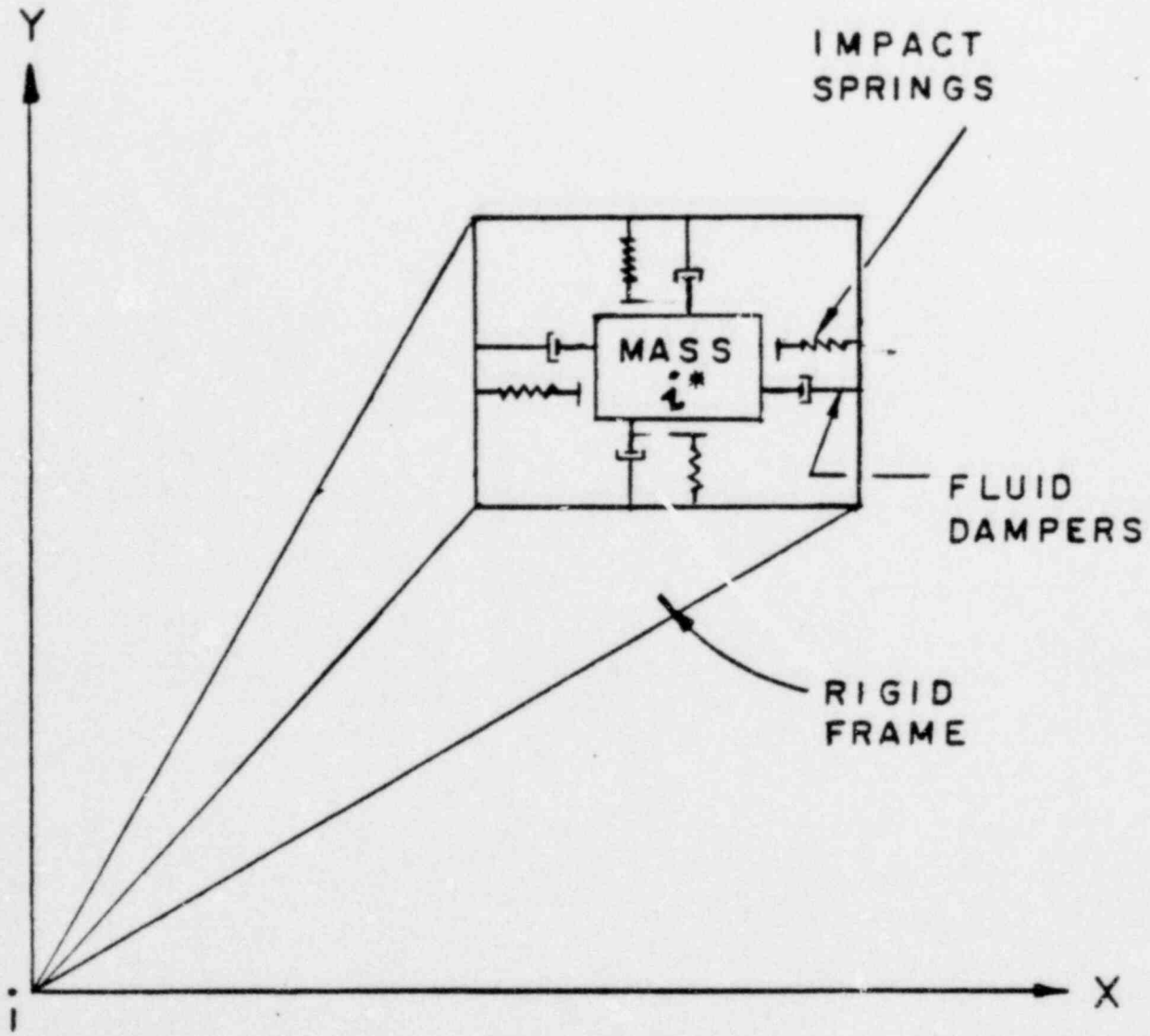

FIG. 6.3 IMPACT SPRINGS AND FLUID DAMPERS

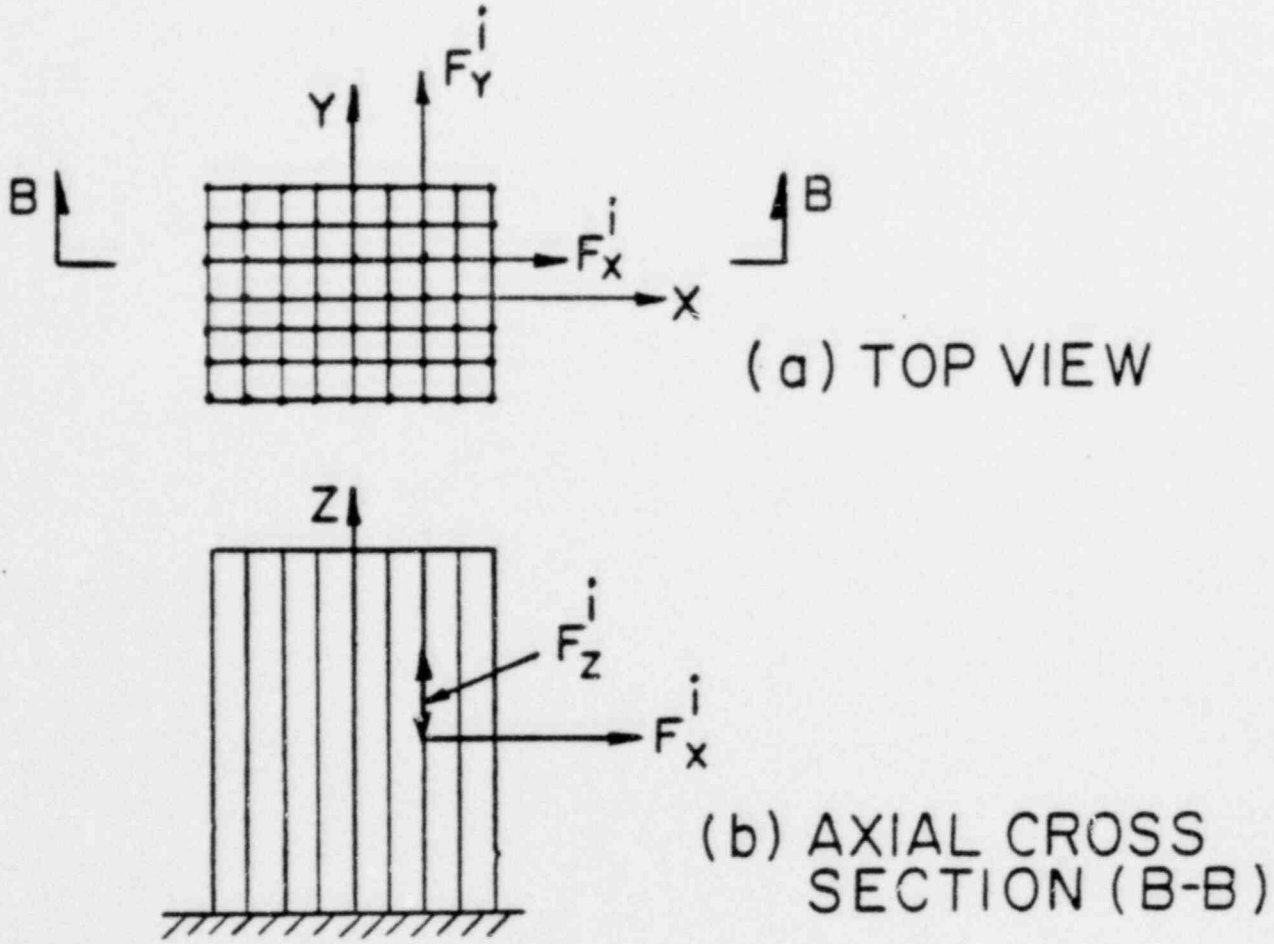

FIG.6.4 (a) HORIZONTAL CROSS SECTION OF RACK
(b) VERTICAL CROSS SECTION OF RACK

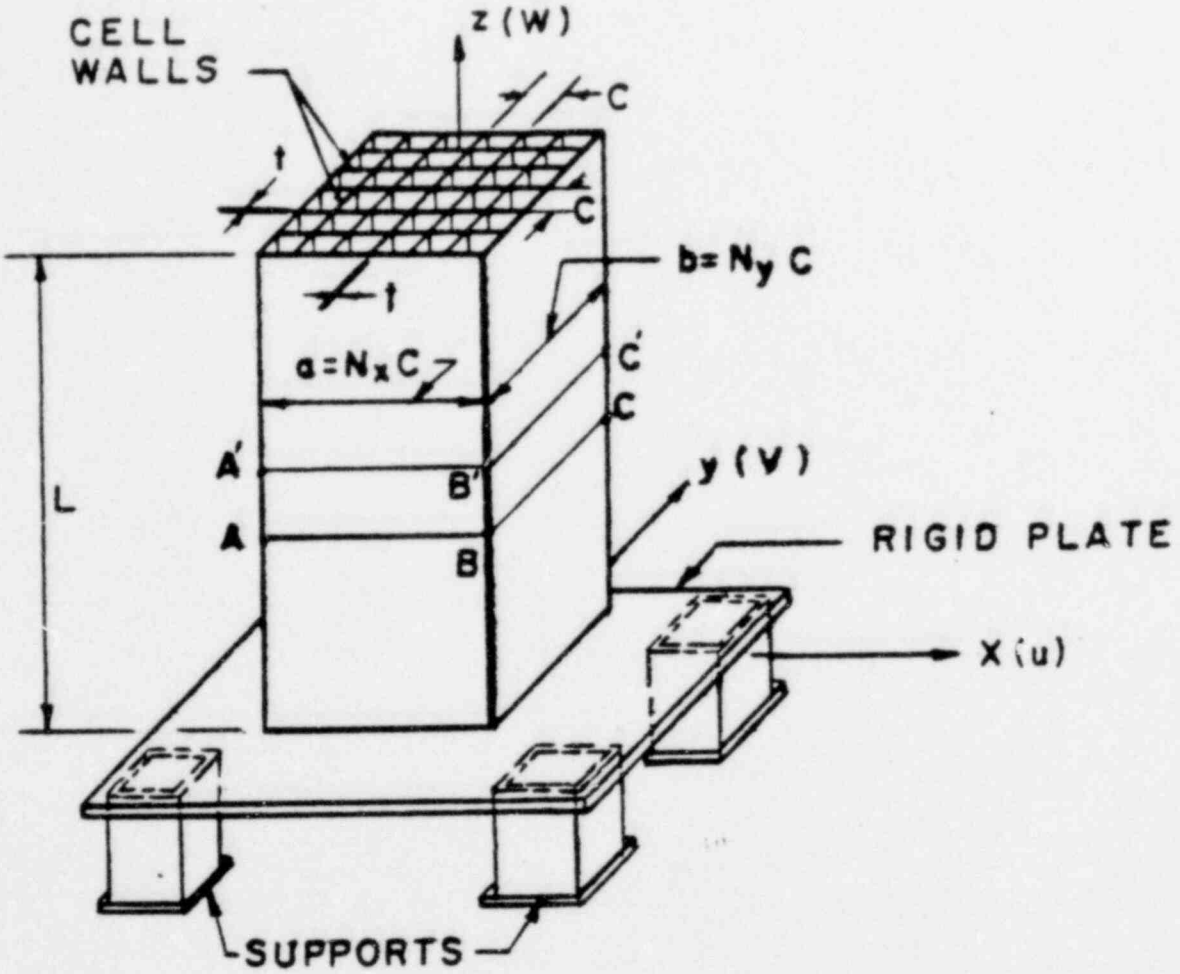
CELL
WALLS
z (W)
C
t
C
b= Ny C
t
a=Nx C
C'
C
A'
B'
y (V)
L
A
B
RIGID PLATE
X (u)
SUPPORTS

FIG. 6.5

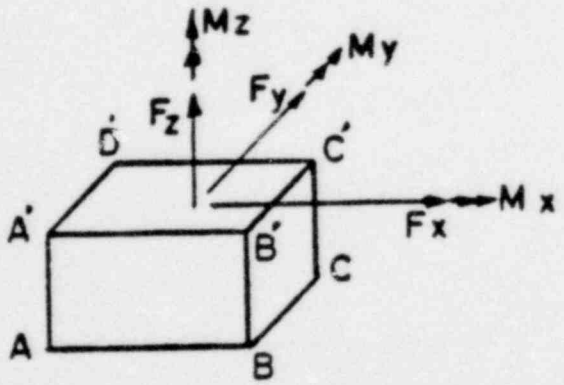
Mz
My
Fy
Fz
D'
C'
Mx
Fx
A'
B'
C
A
B

FIG. 6.6

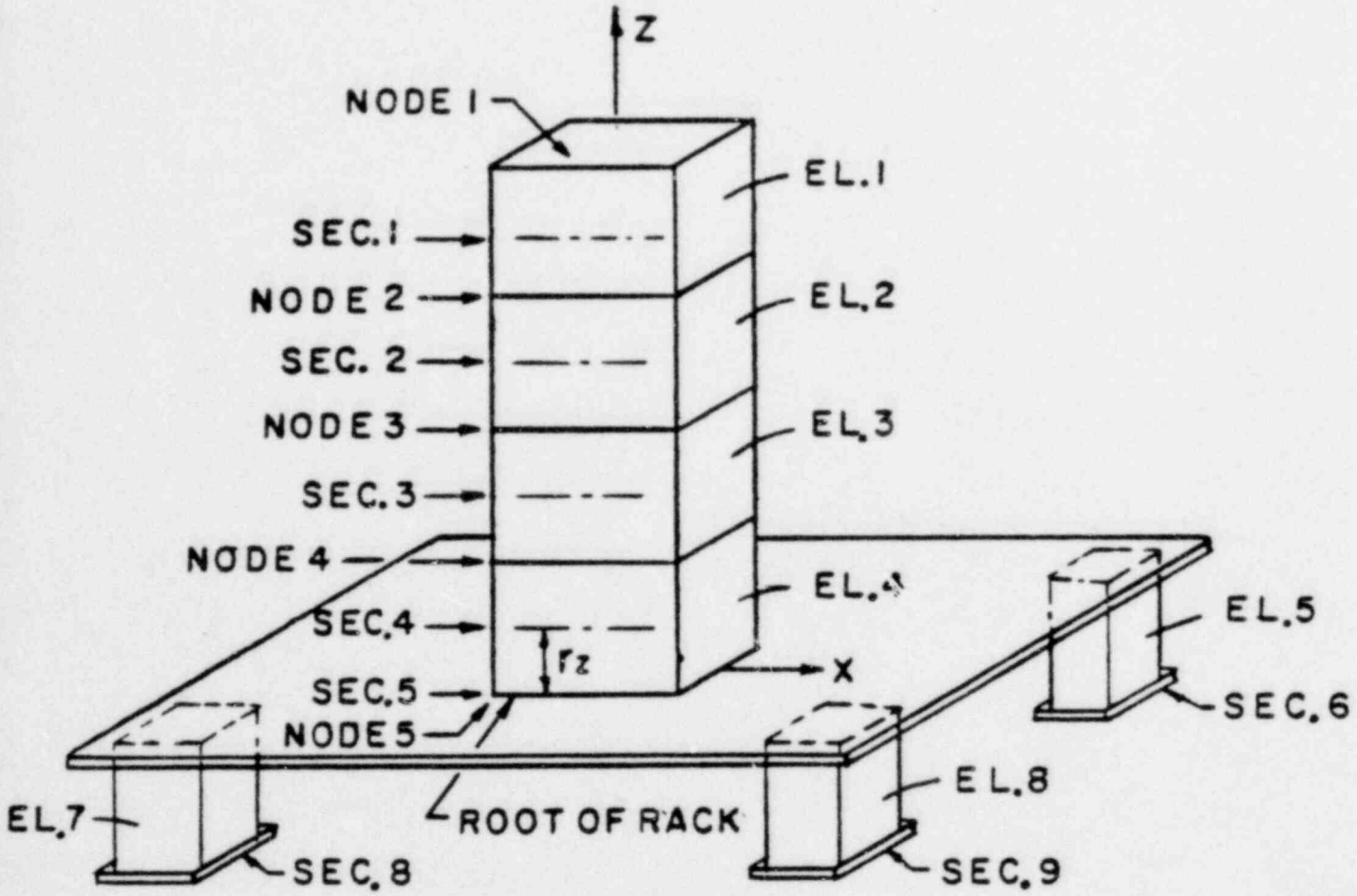

NO. OF ELEMENTS = 8
NO. OF SECTIONS = 9
NO. OF NODES = 5

FIG. 6.7

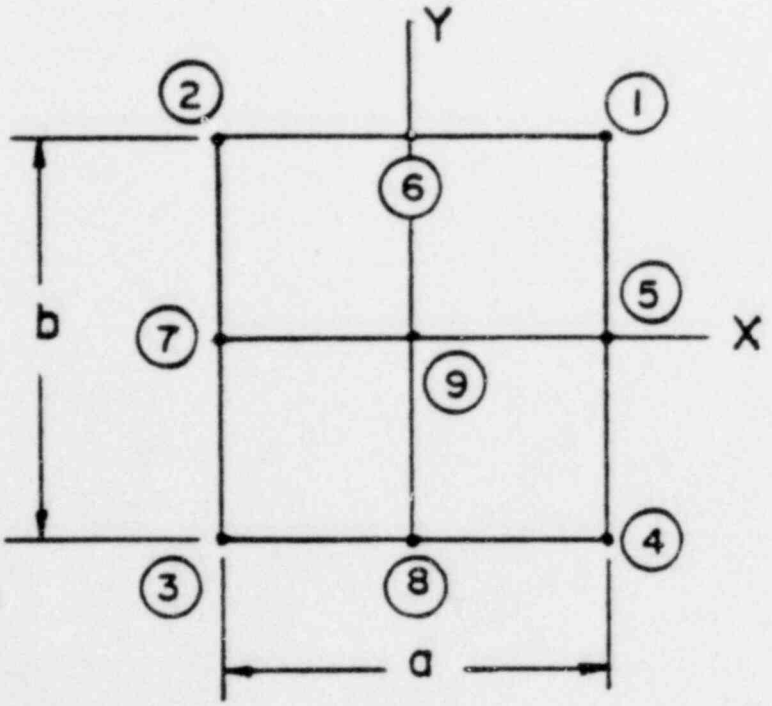

FIG. 6.8

References to Section 6

1. Regulatory Guide 1.29, Seismic Design Classification, Rev. 2, Feb. 1976.

2. "Friction Coefficients of Water Lubricated Stainless Steels for a Spent Fuel Rack Facility", by Prof. Ernest Rabinowicz, M.I.T., a report for Boston Edison Company.

3. Regulatory Guide 1.92, Combining Modal Responses and Spatial Components in Seismic Response Analysis, Rev. 1, Feb. 1976.

   Regulatory Guide 1.61, Damping Values for Seismic Design of Nuclear Power Plants, Oct. 1973.

4. "The Component Element Method in Dynamics with Application to Earthquake and Vehicle Engineering" by S. Levy and J.P.D. Wilkinson, McGraw Hill (1976).

5. General Electric specification 22A5866, Rev. 1, Appendix II, Fuel Assembly Structural Characteristics.

6. R.J. Fritz, "The Effect of Liquids on the Dynamic Motions of Immersed Solids", Journal of Engineering for Industry, Trans. of the ASME, Feb. 1972, pp. 167-173.

7. "Seismic Analysis of Quad Cities High Density Racks, Oat report No.(later).

8. J.T. Oden, Mechanics of Elastic Structures, McGraw-Hill, N.Y., 1967.

9. R.M. Rivello, Theory and Analysis of Flight Structures, McGraw-Hill N.Y., 1969.

10. M.F. Rubinstein, Matrix Computer Analysis of Structures, Prentice-Hall, Eaglewood Cliffs, N.J., 1966.

11. J.S. Przemienicki, Theory of Matrix Structural Analysis, McGraw-Hill, N.Y., 1966.

12. P. Kuhn, Stresses in Aircraft and Shell Structures, McGraw-Hill, N.Y., 1956.

13. S.P. Timoshenko and J.N. Goodier, Theory of Elasticity, McGraw-Hill, N.Y., 1970, Chap. 10.

14. U.S. Nuclear Regulatory Commission, Standard Review Plan, NUREG-75/087, Section 3.8.4.

15. SRP NUREG-75/087, Section 3.8.5.

16. NRC Regulatory Guide 1.124.

7. MISCELLANEOUS ANALYSES

In addition to the ground motion analyses, the following mechanical loads are analyzed:

a. Dropped Fuel Accident I

A fuel assembly (weight - 600 lbs.) dropping from 36" above a storage location and impacting the base. Local failure of the base plate is acceptable; however, a substantial impact with the pool liner is not allowed. The sub-criticality of the adjacent fuel assemblies is not be violated.

b. Dropped Fuel Accident II

One fuel assembly dropped from 36" above the rack and hits top of rack. Permanent deformation of the rack is allowed but is required to be limited to the top region such that the rack cross-sectional geometry at the level of the top of the active fuel (and below) is not altered.

c. Jammed Fuel Handling Equipment and Horizontal Force

A 2000 lb. uplift force and 1000 lb. horizontal force applied at the top of rack at the "weakest" storage location. The force is assumed to be applied on one wall of the storage cell boundary as an upward shear force. The damage, if any, is required to be limited to the region above the top of the active fuel.

The above loading conditions are analyzed to determine an upper bound on the plastic deformation zones. It is shown that the plastic deformation is limited to the rack structure well removed from the active fuel regions. Thus the subcriticality of the fuel arrays is not modified or violated.

10. NEUTRON ABSORBER MATERIAL

The material utilized for neutron attenuation in the racks is Boraflex; a proprietary product of Bisco, a Division of Brand Industrial Services. This material is available in sheet form which facilitates easy handling and a close control of lateral dimensions during fabrication. This material has found widespread acceptance due to its durability, and a remarkable retention of physical and mechanical properties when subject to high or low flux irradiation under typical fuel pool environments. A brief resume' of the established information on this material is given in the following:

10.1 Chemical Composition

The elemental composition of the Boraflex proposed can be divided into two catagories, the polymeric matrix system and the boron carbide power. The elemental composition of each to the nearest 0.5 wt. % is listed below:

TABLE I

Elemental Composition of Boraflex Components by Weight %

ELEMENT	POLYMER	B_4C
Silicon	41%	-
Oxygen	37%	-
Hydrogen	4.5%	-
Carbon	17.5%	23.5%
Boron	-	76%
Iron; soluble borons	-	0.5%

The minimum B^{10} loading is 0.014 grams/cm^2 at a nominal thickness of .070". The criteria suggests a formulation based on 42 wt. % boron carbide to assure that the specified B^{10} content is exceeded at the minimum acceptable manufacturing tolerance thickness ($\pm$ 10% typical, $\pm$ .010" maximum). The elemental content of Boraflex based on this formulation would be as follows:

TABLE II

Elemental Composition of Boraflex Containing 42 wt. % B_4C (by wt. %)

Silicone	24.0%
Oxygen	21.5%
Hydrogen	2.5%
Carbon	20.0%
Boron	32.0%

Iron, soluble boron - trace

Note that the isotopic B^{10} content expressed as wt. % of total boron is typically $18.0 \pm .4$.

10.2 Physical Properties

Boraflex has been extensively tested for physical and mechanical characteristics when subjected to high and low rate irradiation while contained in air, deionized water or borated water environments. Careful laboratory data on neutron attenuation, elemental boron leaching, residual activity, gas generation, etc. were also taken and documented. Bisco report 748-10-1 contains detailed description of the procedures and recorded results. It is shown that the exposure of boraflex in air to 2.81×10^8 rads gamma from a spent fuel source results in no significant physical changes nor in the generation of any gas. Irradiation to the level 1.03×10^{11} rads gamma with a substantial concurrent neutron flux in air, deionized water, and borated water environments causes some increase in hardness and tensile strength of boraflex. During that irradiation a certain amount of gas is generated but beyond the level of 1×10^{10} rads gamma it drops off considerably. The rate of gas generation is found to be greater when B_4C is irradiated in deionized or borated water in absence of boraflex, thus confirming the function of boraflex polymer as our escapsulant which mitigates the interaction between boron carbide and the environment. Vent holes are provided on top of each storage cell compartment to eliminate gas entrapment.

Measurements of the specimen width, thickness, weight, specific gravity at pre- and post-irradiation stages indicated minuscule variation in these quantities.

Experiments also show that neither irradiation, environment or boraflex composition has any discernible effect on the neutron transmission of boraflex. Tests also prove that boraflex does not possess leachable halogens that may be extracted into the pool environment in the presence of radiation. Similar conclusions are reached regarding leaching of elemental boron out of boraflex.

11. IN-SERVICE SURVEILLANCE PROGRAM FOR BORAFLEX NEUTRON ABSORBING MATERIAL

11.1 Program Intent

A sampling plan to verify the integrity of the neutron absorber material employed in the high density fuel racks in the long-term environment is described in this section.

The program is intended to be conducted in a manner which allows access to representative absorber material samples without disrupting the integrity of the fuel storage system. The program is tailored to evaluate the material in normal use mode, and to forecast future changes using the data base developed.

11.2 Description of Specimens

The absorber material, henceforth referred to as "poison" used in the surveillance program must be representative of the material used within the storage system. It must be of the same composition, produced by the same method, and certified to the same criteria as the production lot poison. The sample coupon must be of similar thickness as the poison used within the storage system and not less than 4" x 4" on a side. Figure 1 showed a typical coupon. Each poison specimen must be encased in a stainless stell jacket of an identical alloy to that used in the storage system, formed so as to encase the poison material and fix it in a position and with tolerances similar to that designed into the storage system. The jacket would be closed by tack welding in such a manner as to retain its form throughout the use period yet allow rapid and easy opening without contributing mechanical damage to the poison specimen contained within.

11.3 Test

The test conditions represent the vented conditions of the cruciform elements. The samples will be located adjacent to the fuel racks and suspended from the spent fuel pool wall. Eighteen (18) test samples are to be fabricated in accordance with Figure 1 and installed in the pool when the racks are installed.

The procedure for fabrication and testing of samples shall be as follows:

a. Samples shall be cut to size and carefully weighed in milligrams;

b. Length, width and average thickness of each specimen to be measured and recorded;

c. Samples shall be fabricated in accordance with Figure 1 and installed in pool;

d. Two samples shall be removed at each time instant per the schedule shown in Table 1.

11.5 Specimen Evaluation

After removal of the jacketed poison specimen from the fuel pool at the designated time, a careful evaluation of that specimen will be made to determine its actual condition as well as its apparent durability for continued function. Separation of the poison from the stainless steel specimen jacket must be performed carefully to avoid mechanically damaging the poison specimen. Immediately upon removal, the specimen and jacket section should be visually examined for any effects of environmental exposure. Specific attention should be directed to the examination of the stainless steel jacket for evidence of physical degradation. Functional evaluation of the poison material is accomplished by the following measurements:

a. A neutron radiograph of the poison specimen will allow for a determination of the maintenance of uniformity of the boron distribution;

b. Neutron attenuation measurements of the specimen made in a fashion consistent with that described in the Poison Material Qualifying Test Data will, by comparing with the attenuation of preirradiated poison as listed in that document, allow evaluation of the continuing nuclear effectiveness of the poison. Consideration must be given in the analysis of the attenuation measurements for the level of accuracy of such measurements as indicated by

the degree of repeatability normally observed by the testing agency;

c. A measurement of the hardness of the poison material will establish the continuance of physical and structural durability. Hardness acceptability criterion requires that the specimen hardness will not exceed the hardness listed in the qualifying test document for lab test specimen irradiated to 10^{11} rads. The actual hardness measurement should be made after the specimen has been withdrawn from the pool and allowed to air dry for not less than 48 hours to allow for a meaningful correlation with the preirradiated sample;

d. Measurement of the length, width and average thickness and comparison with the pre-exposure data will indicate dimensional stability within the variation range reported in the Boraflex laboratory test reports.

A detailed procedure paraphrasing the spirit of this program is prepared for step-by-step execution of the test procedure and interpretation of the test data.

TABLE 1

Date Installed_____

	SCHEDULE	INITIAL WEIGHT (mg/Cm^2-Yr)	FINAL WEIGHT (mg/Cm^2-Yr)	WEIGHT CHANGE (mg/Cm^2-Yr)	PIT PENETRATION mil/Yr
1					
2	90 day				
3					
4	180 day				
5					
6	1 year				
7					
8	5 year				
9					
10	10 year				
11					
12	15 year				
13					
14	20 year				
15					
16	30 year				
17					
18	40 year				

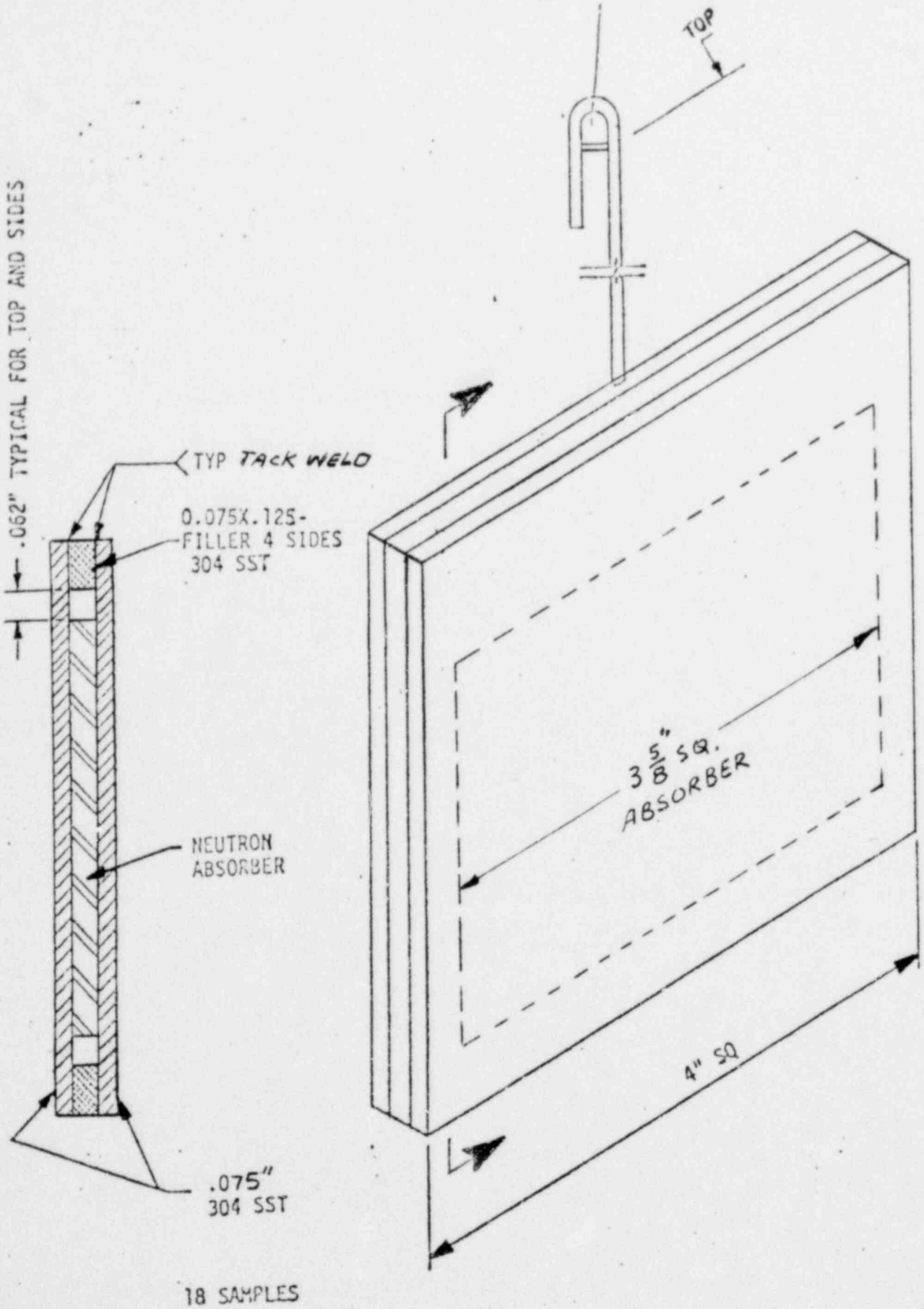
TOP
.062" TYPICAL FOR TOP AND SIDES
TYP TACK WELD
0.075X.125-
FILLER 4 SIDES
304 SST
NEUTRON
ABSORBER
3 5/8" SQ.
ABSORBER
4" SQ
.075"
304 SST
18 SAMPLES

Figure 1.